



**HAL**  
open science

## Dimensional measurement of TiO<sub>2</sub> (Nano) particles by SAXS and SEM in powder form

Najoua Bouzakher-Ghomrasni, Olivier Tache, Jocelyne Leroy, Nicolas Feltin, Fabienne Testard, Carine Chivas-Joly

### ► To cite this version:

Najoua Bouzakher-Ghomrasni, Olivier Tache, Jocelyne Leroy, Nicolas Feltin, Fabienne Testard, et al.. Dimensional measurement of TiO<sub>2</sub> (Nano) particles by SAXS and SEM in powder form. *Talanta*, In press, 234, pp.122619. 10.1016/j.talanta.2021.122619 . cea-03274569

**HAL Id: cea-03274569**

**<https://cea.hal.science/cea-03274569>**

Submitted on 30 Jun 2021

**HAL** is a multi-disciplinary open access archive for the deposit and dissemination of scientific research documents, whether they are published or not. The documents may come from teaching and research institutions in France or abroad, or from public or private research centers.

L'archive ouverte pluridisciplinaire **HAL**, est destinée au dépôt et à la diffusion de documents scientifiques de niveau recherche, publiés ou non, émanant des établissements d'enseignement et de recherche français ou étrangers, des laboratoires publics ou privés.

# Dimensional measurement of TiO<sub>2</sub> (Nano) particles by SAXS and SEM in powder form

Najoua Bouzakher-Ghomrasni<sup>a</sup>, Olivier Tache<sup>b</sup>, Jocelyne Leroy<sup>b</sup>, Nicolas Feltin<sup>a</sup>, Fabienne Testard<sup>b</sup>, Carine Chivas-Joly<sup>a</sup>

*a. Laboratoire National de métrologie et d'Essais – Nanometrology - CARMEN Platform, 29 avenue Hennequin, 78197 Trappes Cedex (France)*

*b. Université Paris-Saclay, CEA, CNRS, NIMBE, 91191, Gif-sur-Yvette, France.*

Corresponding authors: [Fabienne.testard@cea.fr](mailto:Fabienne.testard@cea.fr) and [Carine.chivas-joly@lne.fr](mailto:Carine.chivas-joly@lne.fr)

**Keyword:** SEM; SAXS; Metrology; (Nano)particles; Manufactured products; TiO<sub>2</sub>.

## Highlights:

- Characterization of TiO<sub>2</sub> nanoparticles in powder form from pristine and manufactured products.
- Comparison of different measurands by using SAXS/BET and SEM analysis for different TiO<sub>2</sub> nanoparticles families to achieve to a dimensional parameter.
- Highlighting the influence of polydispersity in shape, interactions and impurities, that can affect the results on size measurement.
- Illustration of the difficulties in comparing size measurement for nanomaterials.

## ABSTRACT:

The market for nano-additive materials has been growing exponentially since 2012, with almost 5040 consumer products containing nanoparticles in 2021. In parallel, the increasing recommendations, definitions and legislations underline the need for traceability of manufactured nanoparticles and for methods able to identify and quantify the “nano” dimensional character in manufactured product. From a multi-technic approach, this paper aims to compare the mesurands extracted from SAX/BET (specific surface area) and SEM (diameter equivalent to a projected surface area) on different TiO<sub>2</sub> powder issued from referenced, synthesized materials, raw materials (additives) and extracted materials from manufactured products. The influence of various parameters such as the anisotropic factor, the interaction between particles, the size distribution and the extraction steps are discussed to illustrate their impact on the diameter values issued from two different measurands. These results illustrate the difficulties in (nano)particles characterization. SEM and SAXS are complementary technics depending on the level of dimensional characterization required.

## 1. Introduction

The nanomaterials development has undergone significant progress over the past thirty years and is now largely used in different domains. To account for traceability of the nanoparticles (NPs) from their production to the end of their cycle life, the need for a neat definition applicable to the different sectors became rapidly an evidence [1]. Since the general nanomaterial definition proposed by the European Commission (EC) in 2011, several definitions from various sources have been laid [2–4]. At the normative level, a nanomaterial was only defined as a material having an external dimension at the nanoscale (ISO/TS 8004) [3]. But a list of parameters essential for the “nano” properties identification and characterization (size distribution, state of agglomeration, shape, specific surface, composition, solubility...) also completed this definition (ISO/TR 13014) [2]. In parallel, different numerous sectoral European legislations have been published to give a definition and a framework for the specific use of nanomaterial, namely, the cosmetics regulation [5], Novel Foods (regarding food products) [6], and the biocide regulation [7]. These definitions are now completed by mandatory annual declarations imposed, first in France in 2013 via the R-Nano register [8] and via the REACH regulation at the European level, since December 2018 [9]. All these recommendations, definitions and legislations underline the need for easy and quantitative characterizations of the nanomaterials in their pristine form or along their life cycle where they are embedded in complex systems. Characterization should provide particle size to classify the materials (in nano or non nano classification) according to the different definitions. It is now admitted that this could only be achieved from a combination of techniques [10–12]. To cite a few: the direct methods like microscopy based techniques provide a measurement of the “geometrical-physical” size, which is directly associated to the SI length unit, the Meter. The ensemble methods like scattering or diffraction (indirect methods) provide a measurement of the size, the aggregation state and the crystalline structure of a large number of statistically representative particles simultaneously. The methods which analyze particles separated by size: the single particle Induced Coupled Plasma–Mass Spectrometry (sp-ICP-MS) allows to fully characterize simultaneously dimension and composition of the analyzed particle. Some articles have highlighted the reliability of SAXS combined to another technique to extract dimensional information on reference particles (from SAXS/Sp-ICPMS couple [13,14] or SAXS/SEM/TEM combination [15]) or on synthesized particles [16,17] or on raw materials [18] (by SAXS/SEM/TEM). Intercomparison SAXS study have also shown that SAXS is an appropriate technique for suspension of monomodal particles under 20nm [19]. The need for such large panel of characterization, including counting, fractionation and spectroscopy have

been underlined by the European NanoDefine project [20,21]. From the NPs size measurement analysis of well-defined controlled materials and industrial materials with complex shape and size, this project have identified some biases in the comparison of techniques based on different principles and physical models. As underlined by NanoDefine project, in highly polydispersed samples, some classical methods are limited for measuring NPs size regarding the EC recommendation. From the JRC report on the identification of nanomaterials [22], it was concluded that only imaging measurements performed with TEM or SEM give direct access to the aggregate constituent particles and the smallest external particle size for a majority of materials, but with a limited number of particles. The comparison of methods for the identification of NPs size in complex matrices is still a matter of debate today.

Among the different NPs used at industrial scale, titanium dioxide ( $\text{TiO}_2$ ) is one of the most important with many applications (Paint, self-cleaning materials, cosmetics and more recently food etc.) [23,24]. Indeed, titanium dioxide is among the five most produced nanoparticle substances (in tonnage), with more than 10,000 tons of  $\text{TiO}_2$  in the nanoparticle state declared in the R-Nano register for the year 2019 [25]. With the increase use of  $\text{TiO}_2$  under NPs form in different domains, demands for identification and regulations start to grow. For example, French Government recently announced the suspension of titanium dioxide (additive  $\text{TiO}_2$ -E171) containing in foodstuffs, for 2020 [26] with an extension to December 2021 [27]. In the different manufactured  $\text{TiO}_2$  nanomaterials, the content of NPs is often not characterized and even changes from one batches to another. An in-depth study of some of the manufactured nanomaterials [28], in particular  $\text{TiO}_2$ -E171, shows a great heterogeneity in the composition of the batches present in the market, in particular with regard to particle size distribution (the percentage in number of particles smaller than 100 nm varies from 11 to 46%) [29]. For 15 different pristine  $\text{TiO}_2$ -E171 batches, Verleysen et al. have identified large variation in size (with a median Feret min diameter between 79 and 149 nm), crystallinity and physico-chemical form, from a combination of TEM and SpICP-MS [30]. Food-grade  $\text{TiO}_2$  particles in manufactured products present a wide particle size distribution and a nanosized tail. A more rigorous characterization of these substances in terms of dimensional characterization and nano fraction quantification is therefore essential, and remains a main challenge for their traceability.

Recently, articles started to describe analyses of  $\text{TiO}_2$  in complex matrices (e.g. food and health care products). Regarding commercial products, 145 products, out of the 5000 declared in the Nanodatabase contain  $\text{TiO}_2$  in nanoparticle form [31]. There is admittedly a strong increase of publications on this subject in the last few years, yet there is a lack of a suitable strategy for  $\text{TiO}_2$  nanomaterials characterization. The identification and dimensional measurement of these NPs could be troublesome without prior sample preparation, an important point highlighted in the literature

(extraction, sonication, zeta potential, pH...). We have recently shown the importance of sample preparation to identify nanomaterials in complex matrix by SEM measurements [32]. First, extraction must be efficient to recover the NPs without transformation and then depending on the characterization tools a step leading to a well dispersed suspension is needed (e.g. for SEM analysis). TiO<sub>2</sub> particles have been detected and quantified in numerous sunscreen matrices by multiple analytical techniques, specifically separatives techniques such as, asymmetric flow field-flow fractionation coupled to inductively-coupled plasma-mass spectrometry (AF4-ICP-MS) [33] or single-particle ICP-MS (spICP-MS) [34,35]. As underline by A. Philippe et al. [36], in the case of TiO<sub>2</sub> particles used in the sunscreens, the multi-technical aspect combination with separation technique and TEM images enabled the determination of constituent particle sizes [36]. I. De La Calle et al. studied with a combination of DLS and AF4-ICP-MS 21 food and beverage products containing NPs (TiO<sub>2</sub>, SiO<sub>2</sub>...) to evaluate the presence of (nano-) particles in their composition [35]. They identified particles with size ranging from 10 nm to 300 nm. Recently, Dufouir et al., focused on four types of chewing gum [37]. For one of them, the coating fraction was 99% pure TiO<sub>2</sub>, while the others were composed by a mixture of TiO<sub>2</sub> with other additives such as calcium carbonate (E170), magnesium silicate (E553a) or talc (E553b). In all these samples, TiO<sub>2</sub> particles were easily identified by a direct microscopy method (TEM) but all these studies evidence the difficult comparison between different measurands associated to different techniques. It is necessary to develop a multi-level approach that combines different reference materials and previous knowledge of the complex material (physico-chemical properties, including morphology of the particles) to fully determine their dimensional characteristic.

Here in this article, we describe a multi-technique approach with direct (SEM) and indirect (SAXS and BET) methods combined to physico-chemical identification analytical tools (X-Ray Photoelectron Spectroscopy (XPS), Energy-Dispersive X-Ray Spectroscopy (EDS), Inductively Coupled Plasma Optical Emission Spectrometry (ICP-OES), zeta potential and X-ray diffraction (XRD)) to determine the size of TiO<sub>2</sub> NPs in a pristine state or issued from complex matrices. The aim of this work is to compare two different measurands used for dimensional characterization: a specific surface area for SAXS and BET and a diameter equivalent to a projected surface area for SEM. Emphasis will be placed on the assessment of the complex matrix, particle size and shape, crystallinity and how characterization method influences dimensional measurements. A metrological challenge is involved in order to characterize TiO<sub>2</sub> particles with various types, shapes, sizes and sources. We will particularly illustrate how the polydispersity in size and interactions between particles are key points for the nanoparticle size identification and we will underline the importance of extraction steps prior to the characterization.

## 2. Material and methods

### 2.1 Material

The different sources of chosen titanium dioxide (TiO<sub>2</sub>) nanoparticles are presented in Table 1. Three families of compounds in powder form have been chosen: synthesized NPs (TiO<sub>2</sub>-Lab), reference NPs (TiO<sub>2</sub>-NM 102 , TiO<sub>2</sub>-NM 104) and particles used as raw materials (TiO<sub>2</sub>-P25 and the food grade TiO<sub>2</sub>-E171) [38,39]. In addition, particles contained in a finished manufactured product from different industrial fields (food, cosmetics, paints and drugs) have been extracted. The sample named TiO<sub>2</sub>-lab was synthesized in the LNE laboratory (synthesis described below), TiO<sub>2</sub>-NM102 and TiO<sub>2</sub>-NM-104 were provided by the Joint Research Centre (JRC), the E171 is a commercial batch raw material and the P25 was purchased from Evonik industries. Four daily use products with TiO<sub>2</sub> nanoparticles were purchased from a local store in Paris in 2019: a pharmaceutical drug (capsules), a sunscreen (SPF 50+), a children's painting and a chewing-gum stick (obtained before the French government suspension). Each of them indicates the presence of the additive TiO<sub>2</sub>-E171 in their formulation.

**Table 1: List of TiO<sub>2</sub> samples used in this research**

N°	Sample	Description	Information on size (electron microscopy) and crystal structure (XRD) from the literature on similar compounds
<i>Reference and synthesized nanoparticles</i>			
1	<b>TiO<sub>2</sub> - Lab</b>	Synthesis of TiO <sub>2</sub> -lab (Stöeber method)	Anatase, 21 ± 6 nm [32]
2	<b>TiO<sub>2</sub>-NM 102</b>	NM102 – Titanium dioxide photocatalytic – Powder JRC*	Anatase, 22 ± 6 nm [15][40]
3	<b>TiO<sub>2</sub>-NM 104</b>	NM-104 Titanium dioxide photocatalytic – Powder JRC*	Rutile, 26 ± 7 nm [15]
<i>Raw materials - Additives</i>			
4	<b>TiO<sub>2</sub>-P25</b>	Aeroxide Evonik P25 – Powder (non-porous mix anatase-rutile phase, surface area 50 m <sup>2</sup> /g) - Evonik Industries)	Anatase/rutile (80/20), wt% Anatase/rutile (28/32) nm crystallite size and 23 ± 9 nm TEM mean diameter [39] [41]
5	<b>TiO<sub>2</sub>-E171</b>	Commercial powder	Anatase, 115 ± 31 - 145 ± 52 nm [39]
<i>Nanoparticles extracted from manufactured products</i>			
6	<b>TiO<sub>2</sub>-Food</b>	Market food (e.g. chewing-gum stick) formulation containing TiO <sub>2</sub> particles	<i>Results for similar batch of chewing-gum stick used in the present study</i> Anatase, 156 ± 61 nm [32]
7	<b>TiO<sub>2</sub>-Drug</b>	Market drugstore formulation containing TiO <sub>2</sub> particles.	No data available
8	<b>TiO<sub>2</sub>-Cosm</b>	Market sunscreen formulation containing TiO <sub>2</sub> particles.	No data available
9	<b>TiO<sub>2</sub>-Paint</b>	Market children's paint formulation containing TiO <sub>2</sub> particles.	No data available

\* Joint Research Centre

## 2.2 Sample preparation

### 2.2.1 TiO<sub>2</sub>-Synthesis

The sample TiO<sub>2</sub>-Lab was synthesized according to an adapted protocol from Marchetti et al. [42]; a 100 mL solution of 0.5 M Titanium (IV) Butoxide (17.51 g at 97%) and 1 M Triethanolamine (15.38 g at 98%) was prepared and heated in the microwave for 10 min at 180°C. The suspension is then centrifuged to recover the solid which is washed 3 times with ultrapure water.

### 2.2.2 TiO<sub>2</sub>-particles extraction

For the commercial products, the NPs embedded in a matrix have to be extracted before their characterization. The extraction method depends on the nature of the matrix studied.

For the gum pellets, the external white layer of eight gum pellets were dispersed in 50 mL of milli-Q® water and placed in an ultrasonic bath for 20 min until complete dispersion. A first centrifugation of the suspension obtained is carried out at 4500 rpm for 20 minutes. The suspension is then washed five times by following these three steps [32]:

- (1) Removal of the supernatant and replacement with milli-Q® water.
- (2) Sonication using an ultrasonic probe, Vibracell 75043 Ultrasonifier (750 W, 20 kHz, Fischer Bioblock Scientific, 13 mm horn), with a 1667 J/mL power (40 % amplitude) for 1 minute (the probe is immersed in a 50 mL beaker filled with water nearby the sample in order to avoid any contamination. The whole setup is surrounded by a 100 mL ice bath to limit overheating due to the energy applied by the probe).
- (3) Centrifugation at 4500 rpm during 20 minutes.

The TiO<sub>2</sub>-Cosm has been treated with another solvent, the dichloromethane, which enables the degradation of the organic matrix. A mass of 3 g of cream was introduced into 20 mL of dichloromethane and the solution obtained is placed in the ultrasonic bath during 20 min for homogenization. Then five washes with dichloromethane were performed according the same steps as for the previous samples.

For the TiO<sub>2</sub>-Paint, the particles were extracted with an acid digestion: A mass of 1.46 g of paint is mixed with 20 mL of hydrogen peroxide (H<sub>2</sub>O<sub>2</sub>) and 1 mL of nitric acid. The obtained suspension is heated until the total evaporation of H<sub>2</sub>O<sub>2</sub> [43]. This first step aims to eliminate the matrix in which the titanium dioxide additive is found. Then five washes with ultra-pure water were realized. The same

protocol was followed on 2 g of paracetamol capsules which have previously been emptied of their active ingredient.

After the washing steps, the particles are redispersed in water (1mL) and then frozen (12 hours) and lyophilized using the freeze dryer Alpha 1-4 LDplus-101541. The analysis is performed under vacuum conditions at 1.65 mbar and -15 °C until obtaining a powder. It should be noted that the powders were handled in compliance with the safety rules associated with nanopowders (mask, gown, under fume cupboard, etc.) [44].

### 2.2.3 Sample preparation for scanning electronic microscopy (SEM)

The powder form of the different samples was suspended in ultrapure water and sonicated with an ultrasonic probe at 1667 J/mL (40% amplitude) for 20 min with a pulsed mode (10 s ON and 10 s OFF) [32]. Then a drop of the suspension was deposited on a silicon wafer substrate using the spin-Coater. A two-stage deposition was required to get a well-dispersed particles layer on the substrate surface. The first one is the spreading phase, where the rotational speed is fixed at 1000 rpm/min with a 500 rpm/min acceleration, for an aqueous solvent, during 60 s. The second step is the drying phase with a rotational speed fixed at 8000 rpm/min during 10 s with a 4000 rpm/min acceleration [45]. In the case of positively charged nanoparticles, the method above was implemented. Otherwise, the substrate was beforehand functionalized by of Poly-L-Lysine (PLL) or Amylamine coating [32,46].

### 2.2.4 Sample preparation for Small angle X-ray scattering (chemSAXS and MOMAC)

For SAXS analysis, the TiO<sub>2</sub> powder is deposited between two sticky kapton separated by a spacer suitable for the SAXS sample holder. As powders doesn't form a compact film, the sample thickness is calculated from the sample optimal transmission knowing its composition (e.g. the density and the X-ray mass attenuation coefficient of the material) [47] (Equation 1) (Figure 1).

$$T = e^{-(\mu \times e_t)} \quad \text{Equation 1}$$

with  $T$  the sample transmission measured by the ratio between incident and transmitted beam;  $\mu$  is the X-ray linear attenuation coefficient in  $\text{cm}^{-1}$  and  $e_t$  the effective thickness in  $\text{cm}$ .

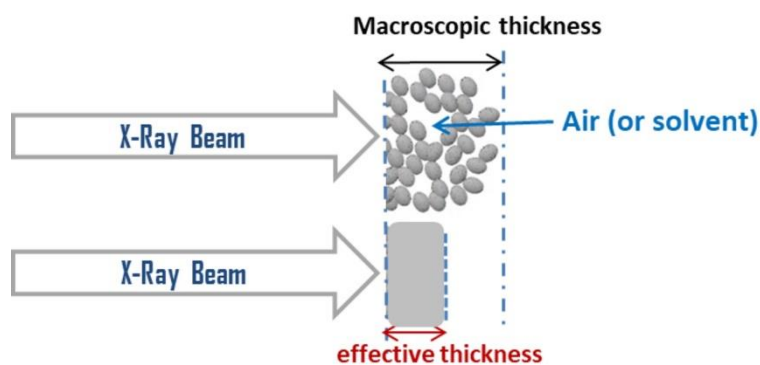


**Figure 1 : Difference between the macroscopic thickness of the powder and the effective thickness of the material constituting the powder (calculated). Inspired from Spalla et al. [47]**

## 2.3 Methods and measurands

### 2.3.1 Scanning Electron Microscopy

#### 2.3.1.1 Acquisition

The measurements in Scanning Electron Microscopy (SEM) were obtained with a Zeiss Ultra-plus SEM equipped with a Field Emission Gun (FEG) and a Gemini column, in the CARMEN platform from the LNE. Brightness and contrast parameters were adjusted to distinguish effortlessly nanoparticles from the substrate background. The resolution claimed by the manufacturer is 1.5 nm at 1 kV and 1 nm at 10 kV. Nanoparticles are deposited on silicon substrates before being analyzed. All images have been carried out through secondary electrons collected by In-Lens detector at 3 KV and with a 3.0 mm working distance. The image resolution has been fixed at  $2048 \times 1536$  pixels.

#### 2.3.1.2 Measurand and statistical analysis

The measurand used for the SEM corresponds to an area-equivalent diameter. For irregular shape NPs, an equivalent diameter is calculated from a projected surface area assuming that the NPs are perfectly spherical. The average diameter,  $D$ , corresponding to the average of area-equivalent diameters as well as the population number-weighted size distribution are determined. The tool used to measure the particle size is Platypus® (see Figure S1), software developed by Pollen Metrology [48]. This software allows the user to measure and count automatically the isolated NPs and/or agglomerate constitutive NPs via an interface control. The constituent NPs within agglomerates require on the contrary manual processing. NPs are measured one by one by adjusting manually an ellipse in each entire particle. Then, the tool determines automatically the particles edge and calculates an area using the pixels number and size inside this edge. All experimental discrete measurements have been fitted to estimate for each  $\text{TiO}_2$ -sample SEM results the parameters of the best probability distribution (see SI 1.). For all the samples, the distributions were best fitted with a log normal law. Table 2 provides the expressions for

the Probability Density Functions (PDF) for the Log-Normal model and statistical parameters estimated regarding the studied particles size (mean diameter (or average size), mode, median (D50), and standard deviations). The repeatability uncertainties related to the measurements ( $u_R$ ) correspond to the standard deviation calculated on average diameters from three different measurements.

**Table 2: Summary of the PDFs for the considered LogNormal model for the size distribution and statistical parameters with  $\mu$  (the expected value or the mean) and  $\sigma$  (the standard deviation) related to the logarithmic values ( $\ln(x)$ ).**

<b>Probability density function of a log-normal distribution</b>	$f_{log\,norm}(x, \mu, \sigma) = \frac{1}{x\sigma\sqrt{2\pi}} e^{-\frac{1}{2}\left(\frac{\ln(x)-\mu}{\sigma}\right)^2}$
<b>Average diameter</b>	$D_{SEM\,average\,area-eq} = e^{\mu + \frac{\sigma^2}{2}}$
<b>Mode</b>	$D_{modal} = e^{\mu - \sigma^2}$
<b>Median (D50)</b>	$D_{median} = e^{\mu}$
<b>Variance</b>	$Var(x) = e^{(\sigma^2 - 1)} e^{(2\mu + \sigma^2)}$
<b>Standard deviation of the size distribution</b>	$SD = \sqrt{e^{(\sigma^2 - 1)} e^{(2\mu + \sigma^2)}} = \sqrt{Var(x)}$

The  $D_{SEM\,average\,area-eq}$  (or mean size) is defined as a number-weighted mean size calculated from the number distribution density. The spread of the size distribution is represented by its variance, which is the square of the standard deviation. The mode of the distribution ( $D_{modal}$ ) is the average size of the most common class. The Median size ( $D_{median}$ ) is the size that divides the distribution into two parts of equal area.

To account for the anisotropy of the particles, The Feret min and Feret max diameters are measured. The Feret diameter ( $D_{Feret}$ ) for a nanoparticle is the distance between the two parallel tangents restricting the object on the opposite sides of the image of a particle as defined by the European project report [49].

### 2.3.2 Small angle X-ray scattering systems (chemSAXS and MOMAC)

#### 2.3.2.1 Acquisition

SAXS (Small Angle X-ray Scattering) experiments were carried out on a home design instrument (chemSAXS) at the SWAXS-Lab platform (CEA Saclay, France) [50]. The X-Ray source (8 keV energy Genix from Xenocs) produces a collimated 0.8 mm x 0.8 mm beam on the sample with an incident flux of  $1 \times 10^8$  photons/s. The sample-to-detector distance is 114 cm resulting in a  $q$  range of  $0.01 \text{ \AA}^{-1}$  to  $0.35 \text{ \AA}^{-1}$  on the detector (Dectris Pilatus 200K). Calibration of the sample-to-detector distance was obtained with tetradecanol while direct beam flux measurements enabled to normalize detector counts into differential cross section per volume following the classical normalization procedures. The absolute scattered intensity normalization is performed by using pySAXS (including

the Kapton windows subtraction), a SAXS data processing software [14,51]. Another set-up MOMAC [52] has been used. It is based on a molybdenum source (17 keV) with a high-flux ( $1.10^8$  photons/s) rotating anode generator. The collimated beam size on the sample is 0.8 mm x 0.8 mm. The sample to detector distance of 63.5 cm results in the 0.03 to 0.8  $\text{\AA}^{-1}$   $q$  range thanks to the use of an XPAD S70 detector. The data processing is identical for both instruments (chemSAXS and MOMAC).

### 2.3.2.2 Data treatment

In order to account for size and shape polydispersity, and the large size range between the different samples, we choose to focus on the large angle signal also called the Porod region to determine the measurand named specific surface, noted  $\Sigma_{\text{Porod}}$  and expressed in  $\text{cm}^{-1}$  ( $\text{cm}^2/\text{cm}^3$ ). An equivalent diameter,  $D_{\text{Porod eq}}$ , is then extracted from this specific surface as described below.

For an infinitely thin interface (in front of the observation scale) between two media of different electronic densities, the intensity at large angles follows a so-called "Porod's law" in  $q^{-4}$  related to the material specific surface (Equation 2) [53,54].

$$\text{Lim Porod} = \lim_{q \rightarrow \infty} Iq^4 = 2\pi \times \Delta\rho^2 \times \Sigma_{\text{Porod}} \quad \text{Equation 2}$$

With,  $I$  the absolute intensity in  $\text{cm}^{-1}$ ,  $q$  the scattering vector in  $\text{cm}^{-1}$ ,  $\Delta\rho$  the scattering length density contrast (difference in scattering length density between the two media) in  $\text{cm}^{-2}$  and  $\Sigma$  is the sample specific surface (ie surface per unit volume) in  $\text{cm}^{-1}$ .

The powders scattering length density is calculated from Equation 3:

$$\rho = \frac{d \times N_A \times Z \times r_e}{M} \quad \text{Equation 3}$$

Where  $d$  is the material density, fixed at  $4.23 \text{ g.cm}^{-3}$  for the rutile phase,  $3.931 \text{ g.cm}^{-3}$  for the anatase phase  $N_A$  is the Avogadro constant with  $N_A = 6.02214 \times 10^{23} \text{ mol}^{-1}$ .  $Z$ , the atomic number.  $r_e$  is the classical radius of the electron ( $r_e = 2.81 \times 10^{-13} \text{ cm}$ ). Lastly,  $M$  is the material molar mass in  $\text{g.mol}^{-1}$ .

For comparison with BET, the specific surface per volume unit,  $\Sigma_{\text{Porod}}$  (in  $\text{cm}^{-1}$ ) are transformed into specific surface per mass unit (or specific surface area, SSA),  $\Sigma_{\text{Porod SSA}}$  (in  $\text{m}^2/\text{g}$ ) as presented in the Equation 4.

$$\Sigma_{\text{Porod SSA}} = \frac{\Sigma_{\text{Porod}} \times 10^{-4}}{d_{\text{material}}} \quad \text{Equation 4}$$

An equivalent diameter ( $D_{\text{Porod eq}}$ ) is defined from the Porod's specific surface,  $\Sigma_{\text{Porod}}$ , assuming a spherical and monodisperse particles shape (Equation 5).

$$D_{Porod\ eq} = \frac{6 \times 10^7}{\Sigma_{Porod}} \quad \text{Equation 5}$$

With,  $D_{Porod, eq}$ , the Porod's equivalent diameter in nm and  $\Sigma_{Porod}$  the specific surface in  $cm^{-1}$ .

### 2.3.3 Brunauer, Emmett and Teller (BET) measurements

The samples specific surface area have been measured by the BET-N<sub>2</sub> adsorption analysis, a method based on an inert gas physical adsorption / desorption on the sample surface. The BET analysis is done in two parts [55,56]. The degassing phase (first part), aims to remove the gas molecules and impurities initially present on the surface of the particles. This step was carried out under vacuum and by first heating at 90 ° C for 1 hour then at 200 ° C for 12 hours. During the second part, the analysis phase, a quantity of adsorbed gas is measured for each relative pressure point (P/P<sub>0</sub>). Adsorption/desorption isotherms are then plotted with the quantity of gas adsorbed (in cm<sup>3</sup>/g) as a function of the relative pressure (P/P<sub>0</sub>) over an interval of 0.01 - 0.99 P/P<sub>0</sub>. From BET analysis, which has been applied to all TiO<sub>2</sub> samples, an external particles specific surface area ( $\Sigma_{BET}$ ) is extracted and an average diameter is defined from  $\Sigma_{BET}$  by assuming the particles are well dispersed and monodispersed, (see SI 6) [57].

### 2.3.4 Chemical composition and physical properties

#### 2.3.4.1 ICP-OES

The samples were mineralized, in the presence of a mixture of suitable acids (i.e. HNO<sub>3</sub>/HCl/HF), in a closed tetrafluoromethoxyl container placed in a microwave oven. Then, the titanium element was quantitatively determined using Plasma emission spectrometry (ICP-OES, HORIBA, Activa M) using a straight-line calibration. The Ti content is given in g per 100g of powder, the conversion into titanium dioxide (TiO<sub>2</sub>) mass contents is then determined by a stoichiometric basis calculation.

#### 2.3.4.2 Elemental composition by Energy-dispersive X-ray spectroscopy (EDS)

Samples elemental composition (atomic composition) can be identified by the Energy-dispersive X-Ray spectroscopy. The detector used in this study is the Ultim® Extreme Windowless 100 mm<sup>2</sup> SDD from OXFORD Instruments. EDS elements mapping are performed at 5 kV beam energy and a 8.5 mm working distance. Elements identification was carried out using the Aztec software.

#### 2.3.4.3 Surface composition by X-Ray photoelectron spectroscopy (XPS)

X-ray photoelectron spectrometry identifies the elements chemical composition present on the surface via the peaks positions testifying to the photoelectrons emission induced by the X-ray and sample interactions. XPS was carried out using a Kratos Axis Ultra DLD spectrometer with a monochromatic

Al K $\alpha$  (1486.6eV) X-ray source and charge compensation system. The take-off angle was set at 90° relative to the sample surface. Spectra were collected using a pass energy of 160 eV for survey and 40 eV for high resolution. The binding energy (BE) scale was calibrated using the Ti 2p<sub>3/2</sub> line at 458.5 eV. The data were analyzed using the CasaXPS software. The peaks fitting were performed after subtracting a mixed Shirley-Tougaard (or Shirley) background. The chemical composition through atomic percentage (at. %) was estimated using peak areas from high resolution spectra. The peak areas were corrected by taking into account the Scofield sensitivity factors.

#### 2.3.4.4 Surface charge and zeta potential

The zeta potential was measured with a Zetasizer Nano ZS (Malvern) for water suspensions with a 0.4 mg/mL concentration. Five measures were realized for each sample and each pH in order to plot the zeta potential curve as a function of the solution pH.

#### 2.3.4.5 X-Ray diffraction (XRD)

Crystalline structures were measured by XRD (PANalytical X'Pert PRO MPD) with a Copper K $\alpha$  radiation wavelength ( $\lambda = 0.15419$  nm). Each TiO<sub>2</sub> sample was performed in the  $\theta$ -2 $\theta$  configuration with a range of angles from 20 to 100° and a measuring step of FWHM/10. XRD patterns were analyzed by HighScore Software. Indeed, each experimental peak represents a crystalline plane which will be compared to a reference pattern (known crystalline material) existing in the PDF-2 database generally supplied with the software (source ICDD, International Center for Diffraction Data). Once the crystal structure is known (rutile or anatase), a crystallite size could be calculated using the Scherrer equation [58].

## **3. Results**

### **3.1 Physico-chemical analysis of selected TiO<sub>2</sub> particles**

The difficulty in the extraction step is to recover a nearly pure sample of TiO<sub>2</sub>-NPs. Essential chemical composition background were analyzed by coupling different techniques. Quantitative inductive coupled plasma with optical emission spectroscopy (ICP-OES) was mainly used to quantify the Ti in the material. XPS was carried out to give direct information on the particles surface local atomic and electronic properties. Semi-quantitative energy dispersive X-ray spectroscopy (EDS)-mapping was carried out on the agglomerated particles in order to determine the chemical composition of the particles and zeta potential have been measured to access to the surface charge in order to complete the surface description. Finally, crystalline structure was determined from X-ray diffraction (XRD). These materials physico-chemical properties are essential for SAXS data processing. Indeed, depending on the chemical nature or crystallinity of the elements present in the powders analyzed, the

densities could varied with an impact on the determination of the specific surface area and the equivalent diameter afterwards.

### 3.1.1 Quantification of Ti element by ICP-OES

The titanium content in the samples was first performed by ICP-OES (Table 3). This analysis enables to check the extraction protocol accuracy after the manufactured product extraction procedure optimization and to analyze the purity of references, synthesized and raw materials. The ICP-OES results show that the samples are of varying purity degrees with a TiO<sub>2</sub> mass percentage ranging from 73 to 97 wt % for the all samples, excepted for TiO<sub>2</sub>-Food which has a low TiO<sub>2</sub> content (25 wt %).

**Table 3 : ICP-OES elemental composition in Ti and TiO<sub>2</sub>, assuming that all detected Ti is in the TiO<sub>2</sub> form (with u, the measurements uncertainties)**

Sample	[Ti] (in g per 100g of powder) ± u	[TiO <sub>2</sub> ] (In g per 100g of powder, wt. %) ± u
<b>TiO<sub>2</sub>-NM102</b>	<b>57.33 ± 2.20</b>	<b>95.64 ± 3.67</b>
<b>TiO<sub>2</sub>-NM104</b>	<b>51.77 ± 1.98</b>	<b>86.35 ± 3.31</b>
<b>TiO<sub>2</sub>-Lab</b>	<b>46.90 ± 1.80</b>	<b>78.24 ± 3.00</b>
<b>TiO<sub>2</sub>-P25</b>	<b>56.97 ± 2.18</b>	<b>95.03 ± 3.64</b>
<b>TiO<sub>2</sub>-E171</b>	<b>58.08 ± 2.23</b>	<b>96.88 ± 3.71</b>
<b>TiO<sub>2</sub>-Paint</b>	<b>55.55 ± 2.13</b>	<b>92.66 ± 3.55</b>
<b>TiO<sub>2</sub>-Cosm</b>	<b>44.36 ± 1.70</b>	<b>73.99 ± 2.84</b>
<b>TiO<sub>2</sub>-Food</b>	<b>15.35 ± 1.00</b>	<b>25.60 ± 1.67</b>
<b>TiO<sub>2</sub>-Drug</b>	<b>58.16 ± 2.45</b>	<b>97.02 ± 4.08</b>

*Tests are performed three times for each sample except for the referenced samples TiO<sub>2</sub>-Food and TiO<sub>2</sub>-Drug, for which only one test was carried out.*

Reference materials TiO<sub>2</sub>-NM102 and TiO<sub>2</sub>-NM104 supposed to be relatively pure contain respectively 96 %wt. and 86 % wt. of TiO<sub>2</sub>. These results are in agreement with ICP-OES JRC results [15] which evidenced trace (0.01-1 %wt.) of minor inorganic impurities for these references. TGA JRC results have also shown the presence of an organic coating on TiO<sub>2</sub>-NM104 which can explain the lower TiO<sub>2</sub> fraction in the presented TiO<sub>2</sub>-NM104 ICP-OES analysis.

For TiO<sub>2</sub>-Lab, results with only 78 %wt. of TiO<sub>2</sub> show the abundant impurities providing from synthesis. For the commercial additive (TiO<sub>2</sub>-P25 and TiO<sub>2</sub>-E171), the analyzed powder is almost pure in TiO<sub>2</sub> (95-97 %wt.) in agreement with the ICP-OES measurements carried out by Dufey et al., on seven different types of food-grade TiO<sub>2</sub>-E171 (97-99 %wt.) and one TiO<sub>2</sub>-P25 (98 %wt.) [39]. For particles extracted from commercial products, small or large quantities of other elements could be incorporated in combination with TiO<sub>2</sub>. Three of the four samples extracted from commercial products (TiO<sub>2</sub>-Paint, TiO<sub>2</sub>-Cosm and TiO<sub>2</sub>-Drug) exhibit a relatively high TiO<sub>2</sub> content (between 74 and 97

% wt.). The case of TiO<sub>2</sub>-Food is particular because the amount of TiO<sub>2</sub> in the extracted powder is very low compared to the other samples (25 % wt.). Dufefoi et al. also evaluated TiO<sub>2</sub> amount in the external coating of four chewing gum brands (with a similar extraction protocol) [37]. Their analyses show a large variation of TiO<sub>2</sub> content in the extracted coating (from 5 to 99 % wt.). In the present case, it seems that the extraction method used did not lead to the complete separation of the TiO<sub>2</sub> particles from the matrix.

### 3.1.2 Chemical surface composition analysis by XPS

The surface composition can be determined by means of XPS spectrum according to the characterizing binding energies of the different elements on TiO<sub>2</sub> particles surfaces. XPS survey spectra from the TiO<sub>2</sub>-NPs (presented in Figure S4) indicate various additional elements summarized in the Table 4 (and Table S3).

For all the TiO<sub>2</sub>-samples, Ti element is retrieved at the surface but in the different samples, residual amounts of adventitious carbon were unavoidable due to their air exposure or contamination. For sample not stored in an inert atmosphere, interactions with CO<sub>2</sub> can take place resulting in an increase of the C element. However, this impurity could also be related to the presence of surface ligands.

**Table 4: XPS chemical surface analysis of TiO<sub>2</sub>-particles in raw materials and extracted from manufactured products**

Sample	Elements (at.%)
TiO <sub>2</sub> - Lab	O (52.9), Ti (19.2), C (23.7), Cl (1.25), N (2.9)
TiO <sub>2</sub> - NM 102	O (50.9), Ti (19.9), C (28.8), S (0.4)
TiO <sub>2</sub> - NM 104	O (45.9), Ti (9.8), C (35.1), Si (0.4), Al (8.8)
TiO <sub>2</sub> - P25	O (39.1), Ti (12.8), C (47.9), Cl (0.3)
TiO <sub>2</sub> -E171	O (44.2), Ti (14.1), C (37.2), K (1.7), P (2.2), Si (0.6)
TiO <sub>2</sub> -Food	O (33.6), Ti (2.1), C (53), Si (2.4), Mg (0.4), Ca (8.5)
TiO <sub>2</sub> -Drug	O (33.1), Ti (10.1), C (54.3), Si (0.7), N (0.9), P (1.1)
TiO <sub>2</sub> -Cosm	O (38.9), Ti (9.1), C (43.7), Cl (0.7), Al (7.7)
TiO <sub>2</sub> -Paint	O (38.1), Ti (9.3), C (48), Si (1.4), P (0.8), Al (2.5)

Ti atomic composition around the surface of the particles (~until 10 nm depth) varied from 2.1 at.% (TiO<sub>2</sub>-Food) to 19.2 at.% (TiO<sub>2</sub>-Lab). The surface composition obtained on reference materials (TiO<sub>2</sub>-NM102 and 104) have been compared to JRC results. Besides the Ti, O and C, other elements were detected on the TiO<sub>2</sub> NM surface. For TiO<sub>2</sub>-NM102, sulfur traces (0.4 at.%) are detected (also reported by ICP-OES but not visible by XPS in the JRC results), but majority of Ti element is measured with an atomic portion of 19.9% compare to 18.6% reported in the JRC report. Concerning TiO<sub>2</sub>-NM104, traces of Si are detected but remain negligible (0.4 at.%) while a considerable amount of Aluminium

(Al) (8.8 at.%) was detected as reported in the JRC study (7.1 at.%). The presence of Al at the surface of NM-104 is explained by a coating layer of Al<sub>2</sub>O<sub>3</sub>.

For TiO<sub>2</sub>-Lab, azote (N) (2.9 at.%) and chloride (Cl) (1.25 at.%) can come from the triethanolamine reactant residue and reactant impurities. The results of TiO<sub>2</sub>-P25 analyses, with a 12.8 at.% of Ti, are slightly below that those reported in the literature (19-20 at.%) [39,59,60]. For the raw material E171, potassium (K) and Phosphate (P) are found on the surface with traces of silicium (Si). The presence of Si is commonly linked to TiO<sub>2</sub> nanoparticles surface treatment, especially for food additives [37,39]. The Ti content around 14 at.% is in the same range order of values (between 12 and 23 at.%) found by Yang et al. on five food-grade TiO<sub>2</sub>-E171 samples [61] or values (14.5 and 23.8 at.%) published by Dufefoi et al. for food-grade E171 [39]. For the extracted component from commercial products, a large proportion of other elements is noticed with a mixture of 11.3 at.% in (Si, Mg and Ca) for TiO<sub>2</sub>-Food, 2.7 at.% in (Si, P and N) for TiO<sub>2</sub>-Drug, 4.7 at.% in (Si, P and Al) for TiO<sub>2</sub>-Paint and 8.4 at.% in (Cl, Al) for TiO<sub>2</sub>-Cosm. Impurities, matrix residue, or specific coating on the extracted TiO<sub>2</sub> particles can explain the presence of such large number of other compounds in coexistence with TiO<sub>2</sub>. Dufefoi et al. and I. De la Calle et al. have also identified other compounds on chewing gum coatings (matrix remnants e.g. MgO, talc, CaCO<sub>3</sub> etc.) [35,37]. In the case of TiO<sub>2</sub>-Cosm, the Cl can come from residual dichloromethane used for the nanoparticles extraction and Al element is frequently detected on the TiO<sub>2</sub>-nanoparticles extracted from sunscreens as a coating layer [36,62]. The presence of phosphorus in some samples could result from the use of anionic surfactants containing polyphosphates during their preparation [63].

This surface chemical analysis revealed the presence of several other elements in addition to TiO<sub>2</sub> (either as a thin layer on the particles surface or as co-existing impurities).

### 3.1.3 Elemental analysis by EDS

EDS provide spatial resolution compositional information. In contrast to XPS analysis, which is mainly sensitive to surface chemical species, EDS analysis is deeper (the depth amount depends on the acceleration voltage and the detected element nature, ~ 200 nm for TiO<sub>2</sub> particles at 5 kV) and provides a better detection of the elements present in the studied sample with the advantage of indicating their location in the particles. EDS-mapping was carried out on the TiO<sub>2</sub>-particles agglomerated/aggregated (Figure S3 A and B). For samples with TiO<sub>2</sub> composition above 74%<sub>w/w</sub> (by ICP-OES), titanium and oxygen corresponds exactly to the location of the TiO<sub>2</sub> particles observed in the SEM images. Consequently, the particles correspond to titanium dioxide composition. Only Ti and O are detected for TiO<sub>2</sub>-NM102 and TiO<sub>2</sub>-P25 particles, which mean that they are pure and uncoated samples (see

Figure S3 A)). TiO<sub>2</sub>-NM104 present a uniform Al particles coating (coming from the Al<sub>2</sub>O<sub>3</sub> coating) which is coherent with XPS analysis. These results are in agreement with EDS analyses performed by the JRC, with a very low presence of Al (500 ppm), Si (800 ppm) and Fe (700 ppm) in addition to TiO<sub>2</sub> for TiO<sub>2</sub>-NM-102 and a small amount of Si (1800 ppm), S (3200 ppm) and larger amount of Al (32000 ppm), in addition to TiO<sub>2</sub> for the TiO<sub>2</sub>-NM-104 particles [15]. For TiO<sub>2</sub>-Lab, nitrogen traces are visible coming from residual nitrogen reactant as identified by XPS. The presence of Chloride identified by XPS is not confirmed by EDS. For the commercial food grade TiO<sub>2</sub>-E171, other elements such as silica, potassium and phosphorus are clearly visible on EDS-mapping around the TiO<sub>2</sub> particles (Figure S3A)). Previous work on the Food-grade E171 reported the presence of the same elements by EDS [30,39]. For the extracted compounds, impurities traces and other elements are identified. For powder extracted from food, where ICP-OES have identified a TiO<sub>2</sub> composition of 25%<sub>w/w</sub>, the SEM-EDS coupling enabled the impurities (Ca and Mg) localization on particles with different morphologies from the TiO<sub>2</sub> ones (Figure S3 B)). These impurities are particles of different nature and can be related to the waxes commonly added on the surface of candies as glazing agent [64]. Additionally, the TiO<sub>2</sub>-Food deposition on a Cu-C grid led to the Si identification on the TiO<sub>2</sub> particle surface. For TiO<sub>2</sub>-Paint and TiO<sub>2</sub>-Drug, all elements detected by EDS mapping are in agreement with the XPS analysis. TiO<sub>2</sub>-Cosm mapping shows the Al element located on the TiO<sub>2</sub> particles. The EDS mapping results obtained in this study are consistent with XPS findings for the presence of several other elements in addition to TiO<sub>2</sub>, but allows to identify coexisting particles of different natures.

### 3.1.4 Surface charge by zeta potential

The particles surface charge can vary from one TiO<sub>2</sub> sample to another, depending on elements present on the surface. The presence of a coating layer has a direct impact on the zeta potential value and thus on the isoelectric point (IEP). It is therefore an indirect way to identify the coating of the nanoparticles in complement to XPS and EDS. Results obtained from TiO<sub>2</sub> samples present different isoelectric points (IEP); 4.5 (NM102), 4 (TiO<sub>2</sub>-P25), 7.4 (NM104, TiO<sub>2</sub>-Paint, TiO<sub>2</sub>-Cosm), 2 (TiO<sub>2</sub>-E171, TiO<sub>2</sub>-Food and TiO<sub>2</sub>-Drug) and 5.3 (TiO<sub>2</sub>-Lab) (Figure S5). The IEP obtained for TiO<sub>2</sub>-NM102, TiO<sub>2</sub>-P25 and TiO<sub>2</sub>-Lab are slightly lower than the expected value for TiO<sub>2</sub> pure surface (between 5 and 6.5 [65]) while, the TiO<sub>2</sub>-Lab IEP is in accordance with a TiO<sub>2</sub> surface IEP. The lower IEP of pH 2 observed for TiO<sub>2</sub>-E171, TiO<sub>2</sub>-Food and TiO<sub>2</sub>-Drug, can be explained by the presence of a silica coating on the surface of these nanoparticles. The higher IEP of pH 7.4 measured for TiO<sub>2</sub>-NM 104, TiO<sub>2</sub>-Paint and TiO<sub>2</sub>-Cosm, could be attributed to an aluminium oxide coating. These results are in agreement with the TiO<sub>2</sub>-EDS-mapping and XPS analysis.

### 3.1.5 Crystallinity by XRD

Structural features are evaluated using XRD patterns. Titanium dioxide exists in three different crystallographic structures: anatase, rutile and brookite. The samples analyzed by XRD (Figure S6) display a variety of crystal structures, with three anatase structure corresponding to TiO<sub>2</sub>-NM-102, TiO<sub>2</sub>-Lab and TiO<sub>2</sub>-E171, three rutile structures with TiO<sub>2</sub>-NM-104, TiO<sub>2</sub>-Paint and TiO<sub>2</sub>-Cosm and a mixture rutile/ anatase structure for the sample TiO<sub>2</sub>-P25. The TiO<sub>2</sub>-Lab with anatase structure presents additional peaks at  $2\theta = 26, 29$  and  $33^\circ$ , which are probably impurities related to reagent residues. TiO<sub>2</sub>-P25 is a mixture sample of both crystalline phases, the proportions of each phase were calculated with the intensities ratio of the most intense peaks for the anatase and rutile phases [66]. Phases mass fraction are about 82 wt%. for anatase structure and 18 wt%. for rutile structure. These values are consistent with the literature [43,67–70].

### 3.2 Size characterization using electron microscopy (SEM)

SEM is a direct imaging method to access to the size distribution, however for complex matrices it requires a preliminary extraction of the nanoparticles prior to the analysis. In a former article [32], the sample preparation have been described in order to demonstrate key points to disperse the particles on the grid (or Si substrate). Using the developed methodology, nine samples have been studied to obtain the size distribution of the constituent particles. The Figure 2 illustrates TiO<sub>2</sub>-samples SEM images of the TiO<sub>2</sub>-particles from raw and extracted materials, and the histogram built from the analysis of a large number of particles (300). In a first approximation, the average diameter is extracted assuming the particles are spherical. Then, to account for the anisotropy, the Feret min and Feret max diameter are extracted. For the majority of samples, the particles are slightly anisotropic, only one presents high anisotropy (TiO<sub>2</sub>-cosm), all of them are are polydisperse in shape and size, as shown by SEM images (Figure 2). The polydispersity in size can be defined as pseudo-spherical particles with broad size distribution.

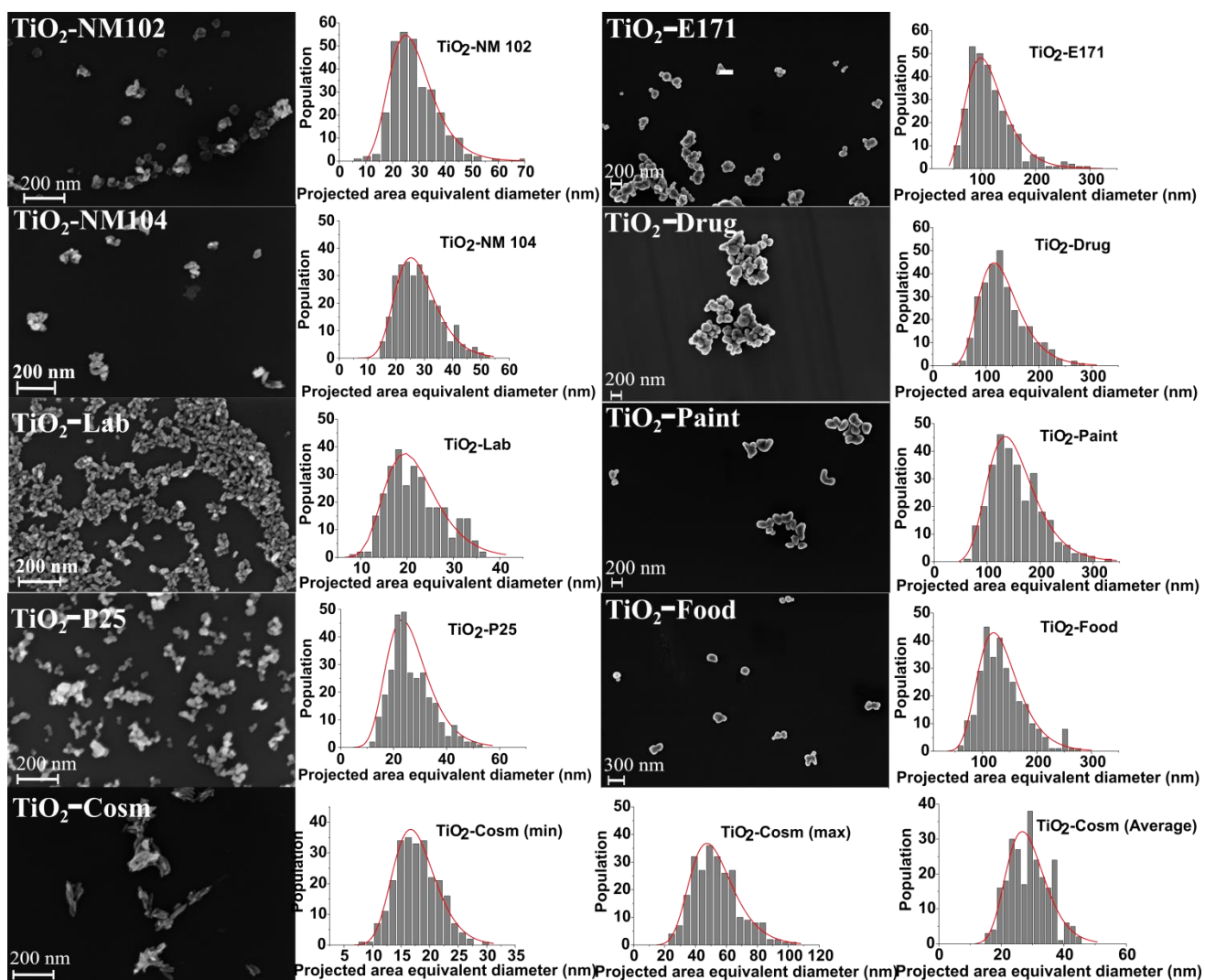


**Figure 2 : Typical SEM images and number weighted size distribution of TiO<sub>2</sub> samples (the red continuous line curve corresponds to one representative statistical distribution modeling reported in table S1 and Figure S2), statistical SEM average results are presented in the Table 5.**

Three series have been achieved for all samples (see details in Table S2). The SEM distribution diameters ( $D_{SEM \text{ average area-eq}}$ ,  $D_{Modal}$ ,  $D_{Median}$ ), and standard deviations of the size distribution are reported in the Table 5. The repeatability uncertainties related to the measurements ( $u_R$ ) correspond to the standard deviation calculated on average diameters from three different measurements. The aspect ratio ( $D_{Feret \text{ min}}/D_{Feret \text{ max}}$ ) was considered to evaluate the anisotropy of the particle.

**Table 5 : Statistical parameters from SEM measurement (average, mode and median diameters each followed by a repeatability uncertainty ( $\pm u_R$ ) over three different number-based distributions performed on the same sample); with  $\mu$ ,  $\sigma$  the mean and the standard deviation of logarithmic values respectively,  $D_{\text{modal}}$  is the average size of the most frequented class,  $D_{\text{median}}$  is the size that splits the distribution into two equal parts of areas.  $F_{\text{min}}$  and  $F_{\text{max}}$  are respectively the maximum and minimum Feret diameters.**

Measurand Sample	$\mu$	$\sigma$	$D_{\text{SEM average area-eq}}$ (nm) $\pm u_R$	Standard deviation of the size distribution	$D_{\text{Modal}}$ (nm) $\pm u_R$	$D_{\text{Median}}$ (nm) $\pm u_R$	Aspect ratio ( $D_{\text{Feret min}}/D_{\text{Feret max}}$ )
TiO <sub>2</sub> -NM 102	3.2	0.4	26.8 $\pm$ 3.1	9.7 $\pm$ 1.7	22.2 $\pm$ 2.4	25.1 $\pm$ 2.8	0.7
TiO <sub>2</sub> -NM 104	3.3	0.3	27.3 $\pm$ 0.5	7.7 $\pm$ 0.8	24.3 $\pm$ 1.0	26.2 $\pm$ 0.7	0.7
TiO <sub>2</sub> -Lab	3.0	0.3	21.1 $\pm$ 0.9	5.8 $\pm$ 0.6	18.9 $\pm$ 0.7	20.3 $\pm$ 0.9	0.8
TiO <sub>2</sub> -P25	3.2	0.3	25.8 $\pm$ 1.2	7.4 $\pm$ 1.4	22.8 $\pm$ 0.7	24.7 $\pm$ 1.0	0.9
TiO <sub>2</sub> -E171	4.6	0.3	110.2 $\pm$ 4.4	37.2 $\pm$ 2.2	93.7 $\pm$ 4.4	104.4 $\pm$ 4.4	0.8
TiO <sub>2</sub> -Drug	4.8	0.4	128.4 $\pm$ 2.1	46.8 $\pm$ 7.7	106.5 $\pm$ 4.9	120.7 $\pm$ 1.8	0.9
TiO <sub>2</sub> -Food	4.8	0.3	133.2 $\pm$ 3.9	43.6 $\pm$ 2.6	114.3 $\pm$ 3.3	126.6 $\pm$ 3.6	0.9
TiO <sub>2</sub> -Paint	4.9	0.4	146.6 $\pm$ 2.5	55.3 $\pm$ 5.9	120.1 $\pm$ 4.8	137.2 $\pm$ 2.8	0.8
TiO <sub>2</sub> -Cosm	3.3	0.2	27.9 $\pm$ 0.9	6.6 $\pm$ 0.4	25.7 $\pm$ 1.2	27.2 $\pm$ 1.0	
TiO <sub>2</sub> -Cosm ( $F_{\text{max}}$ )	3.9	0.3	51.9 $\pm$ 1.0	14.9 $\pm$ 0.4	46.1 $\pm$ 1.3	49.9 $\pm$ 1.1	0.3
TiO <sub>2</sub> -Cosm ( $F_{\text{min}}$ )	2.7	0.2	15.8 $\pm$ 2.8	3.9 $\pm$ 0.1	14.5 $\pm$ 3.0	15.4 $\pm$ 2.8	

For the reference materials, they contain 100% of nanoparticles and the  $D_{\text{SEM average area-eq}}$  for TiO<sub>2</sub>-NM-102 and TiO<sub>2</sub>-NM-104 are respectively, 26.8  $\pm$  3.1 nm and 27.3  $\pm$  0.5 nm. These values fall within the uncertainties range given in the JRC report regarding these two references (21  $\pm$  10 nm for TiO<sub>2</sub>-NM-102 and 26  $\pm$  10 nm for TiO<sub>2</sub>-NM-104) measured by TEM. More, TiO<sub>2</sub>-Lab synthesized has a  $D_{\text{SEM average area-eq}}$  of 21.1  $\pm$  0.9 nm very close to 21.4  $\pm$  6.4 nm obtained by the same process as Ghomrasni et al. [32]. In accordance with previous works with 100% of nanoparticles [39,71], the TiO<sub>2</sub>-P25 average size measured by electron microscopy is equal to 25.8  $\pm$  1.2 nm.

The food grade TiO<sub>2</sub>-E171 has been the subject of several characterization studies, including W. Dufey et al., who characterized seven different batches of TiO<sub>2</sub>-E171, purchased from different suppliers, by TEM [39]. Mean equivalent diameters, derived from TEM distributions, range from 115 (with a size distribution standard deviation of 31 nm) to 145 (with a size distribution standard deviation of 52 nm), which are in agreement with the  $D_{\text{SEM average area-eq}}$  (110.2  $\pm$  4.4 nm) found in this study. Weir et al. [43] underline a very broad size distribution of the additive E171 (30 to 400 nm) with a particles mean diameter around 110 nm and 36% of the particles smaller than 100 nm, in accordance with the size and the 47% fraction of the TiO<sub>2</sub>-E171 particles smaller than 100 nm found in our study. On the other hand, the “Nano” fractions vary from one additive batch to another as demonstrated by E. Verleysen et al. In their work, 15 raw materials from E171 with a majority of Anatase crystallographic

structure were studied [30]. The average sizes measured by TEM (with a median  $D_{\text{Feret Min}}$ ) are between 79 and 149 nm with a nanometric fraction ranging from 18 to 74%. Particles extracted from commercial products, i.e. TiO<sub>2</sub>-Food, TiO<sub>2</sub>-Drug and TiO<sub>2</sub>-Paint, have the same morphology as the food grade additive TiO<sub>2</sub>-E171. After the extraction procedure, the determined  $D_{\text{SEM average area-eq}}$  for TiO<sub>2</sub>-Food, TiO<sub>2</sub>-Paint, TiO<sub>2</sub>-Drug, are respectively  $133.2 \pm 3.9$  nm;  $146.6 \pm 2.5$  nm and  $128.4 \pm 2.1$  nm. Analyses confirmed the presence of nanosized particles in the fraction of 22% for TiO<sub>2</sub>-Food, 17% for TiO<sub>2</sub>-Paint and 29% for TiO<sub>2</sub>-Drug. The obtained results for TiO<sub>2</sub>-Food extracted from chewing gum are in agreement with the TEM average size of 135 nm (with a nanoparticles fraction of 19%) found by Dufefoi et al. on the additive E171 extraction and its dimensional characterization in food products (e.g. chewing gum)[37]. This range of order was also retrieved by Geiss et al. [64] for pristine E171 additives (83-139 nm average size and 23–66% by number of nano-sized constituent particles) and comparable TiO<sub>2</sub>-particles extracted from food products (83 to 122 nm average size with 32-58% nanoparticle fraction). For TiO<sub>2</sub>-particles extracted from pharmaceutical products, Faust et al. [72] revealed by TEM analysis that the extracted samples contained between 32 and 58% of nanoscaled constituent particles with primary particle sizes between  $94 \pm 25$  nm and  $119 \pm 39$  nm, in good agreement with the  $D_{\text{SEM average area-eq}}$  of TiO<sub>2</sub>-Drug ( $128.4 \pm 2.1$  nm).

For the TiO<sub>2</sub>-Cosm sample, The  $D_{\text{SEM average area-eq}}$  is equal to  $27.9 \pm 0.9$  nm. However, TiO<sub>2</sub>-Cosm is different in shape, since it is anisotropic nanoparticles (rods, with an aspect ratio equal to 0.3),  $D_{\text{Feret min}}$  and  $D_{\text{Feret max}}$  have been also measured. The value obtained in the lower dimension is  $15.8 \pm 2.8$  nm. This is in good agreement with other studies such as Philippe et al. [36] that report a panel of eleven sunscreens pseudo-spherical, ellipsoidal or elongated particles shape like those observed for TiO<sub>2</sub>-Cosm with a  $D_{\text{Feret min}}$  evaluated at  $7.3 \pm 2.5$  up to  $31.5 \pm 12.6$  nm.

The samples studied are polydispersed particles mixtures with different shapes and broad size distribution, even within same TiO<sub>2</sub> molecular crystallographic structures. The average size diameter evaluated corresponds to the diameter estimated from a projected surface area ( $D_{\text{SEM average area-eq}}$ ); excepted when the aspect ratio is high. This is the case for TiO<sub>2</sub>-Cosm, where two visible dimensions ( $D_{\text{Average Feret min}}$  and  $D_{\text{Average Feret max}}$ ) were measured to answer to the regulation (figure S2). Microscopy techniques need an optimized dispersion protocol to achieve a well done particles separation and require the total removal of all matrix components from manufactured products. To go in depth, ensemble techniques such as SAXS and BET have been used to access to the external particle dimensions by taking into account irregular particle shape and size polydispersity.

### 3.3 Size characterization using SAXS

#### 3.3.1 Influence of thickness and compactness for SAXS measurements

For SAXS analysis, the thickness of the sample is an important parameter to normalize the intensity and extract the specific surface mesurand. To process the data for powder in the form of grains in contact with air, only the signal that originates from the pure material is considered and thus the pure material thickness (as shown in Figure 1 and detailed in Material and method part) [47]. With an X-ray beam at 8 keV, (Figure 3 a) right) clearly shows the high sensitivity of the normalized intensity with the sample transmission (Figure 3 a) left), when curves should be superimposed. This is related to the inhomogeneity in thickness and compactness in the same pellet which leads to measurement errors (Figure S8). These parameters have to be controlled for a correct absolute intensity measurement.

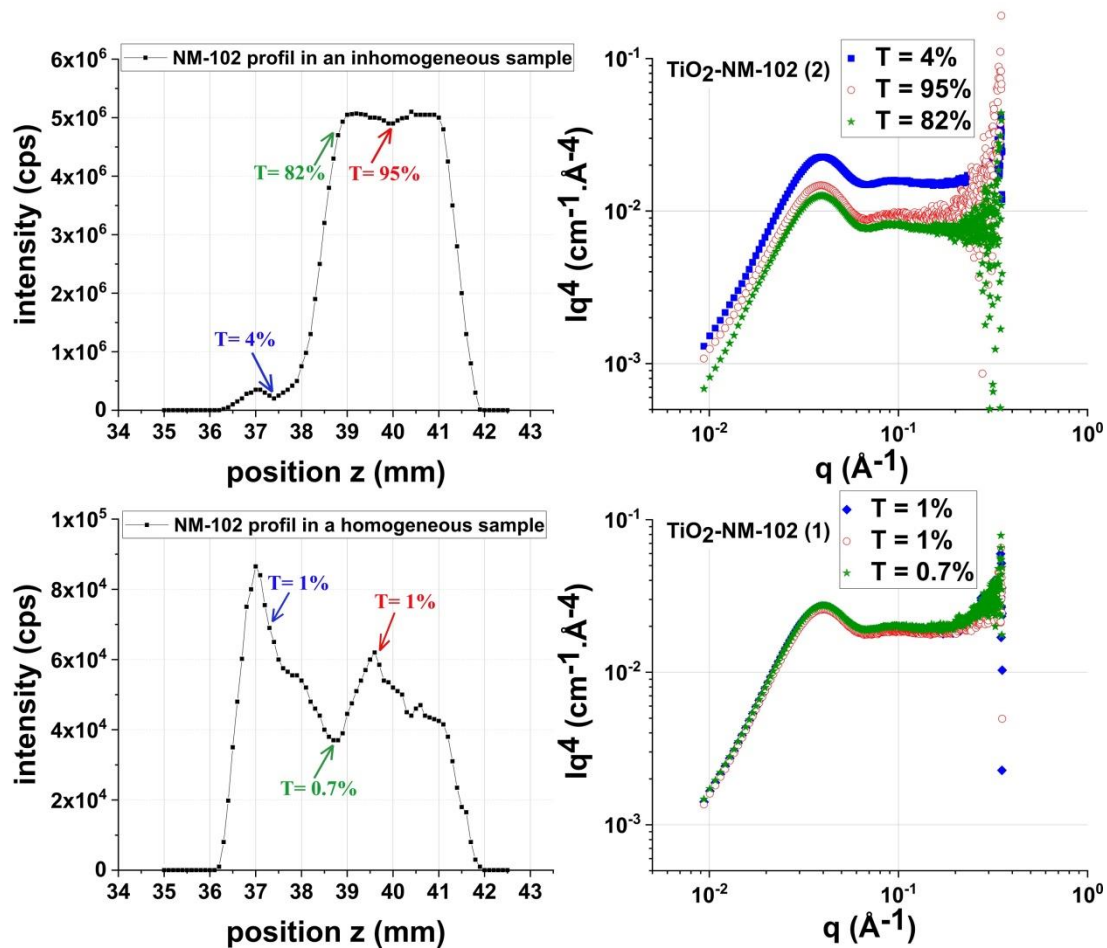


Figure 3 : TiO<sub>2</sub>-NM 102 a) inhomogeneous sample and b) homogeneous sample with, the transmitted intensity (in counts per second “cps”) profile as a function of position z (left) and different curves obtained for different transmissions (at different positions in the sample) (right)

At 8keV, absorption is strong and TiO<sub>2</sub> sample should be very thin (between 0.0026 and 0.0028 cm for a 30% transmission) which can be a high source of error for powder analysis. Figure 3 a) left) presents the variation in transmitted intensity along the pellet. The large amplitude of the measured profile can

explain the variation in the normalized intensity in contrast to the homogeneous sample which exhibits uniform transmission along the pellet (~1%) (Figure 3 b) left) resulting in superimposed SAXS curves (Figure 3 b) right). To overcome the strong absorption of 8 keV X-ray beam, a more energetic and penetrating X-ray beam was used to analyze the TiO<sub>2</sub>-NM102 compact pellet.

The results are presented in Table 6, following the data treatment presented in material and method part.

**Table 6 : SAXS measurements for several transmissions achieved with chemSAXS and MOMAC set-up. Results obtained for TiO<sub>2</sub>-NM 102 sample.**

Set-up	Transmission	Thickness (μm)	Porod's lim (cm <sup>-1</sup> .Å <sup>-4</sup> )	Σ <sub>Porod</sub> (cm <sup>-1</sup> )	Σ <sub>Porod SSA</sub> (m <sup>2</sup> /g)	D <sub>Porod eq</sub> (nm)
chemSAXS 8keV (inhomogeneous sample)	95.5%	1.4	0.0093	1472917	37.5	40.7
	82.0%	4.6	0.0079	1246860	31.7	48.1
	4.3%	72.0	0.015	2426045	61.7	24.7
chemSAXS 8keV (homogeneous sample)	1.1%	100.0	0.018	2860017	72.8	21.0
	0.7%	120.0	0.020	3087178	78.5	19.4
	1.1%	100.0	0.019	3022500	76.9	19.9
MOMAC 17keV (homogeneous sample)	62.0%	86.0	0.019	3002466	76.4	20.0

The measurand (specific surface) is extracted from the asymptotic Porod's limit (Equation 2) measured from the Iq<sup>4</sup> plot shown in Figure 3 (right). Concerning the first preparation (inhomogeneous pellet), the chemSAXS results are very far apart and vary significantly depending on the positions analyzed (associated to different transmission values). Indeed the equivalent diameter ranges from 24.7 to 48.1 nm. On the other hand, for the homogeneous and compact pellet, the chemSAXS results are very close from one point to others (D<sub>Porod eq</sub> = 19.4 - 20.0 nm) and match with MOMAC analysis (see Figure S9 for the comparison of scattering intensity from both set-ups). For SAXS powder analysis, the sample homogeneity and compactness verification is necessary for reliable results [47].

### 3.3.2 Specific surface area and equivalent diameter extracted from SAXS measurements

The same methodology (detailed above) has been applied for the nine samples and the Figure 4 gathered the obtained Porod representation. All samples present the characteristic Porod behavior in the large q range and the specific surface area of each sample is calculated from the Porod's limit (as described in the 2.3.2 section). The Porod limit is clearly defined on a large q range for the references and the synthesized materials while for additive E171 and the extracted powder (TiO<sub>2</sub>-Drug, TiO<sub>2</sub>-Food, TiO<sub>2</sub>-Paint and TiO<sub>2</sub>-Cosm) the Porod plateau extend on a limited q range with a decrease of the signal to noise ratio above (q > 10<sup>-1</sup> Å<sup>-1</sup>). This has to be related to the larger size of the extracted

particles which gives a lower specific surface and thus a lower Porod limit. The Porod limit used to extract the specific surfaces are indicated in dashed line on the Figure 4.

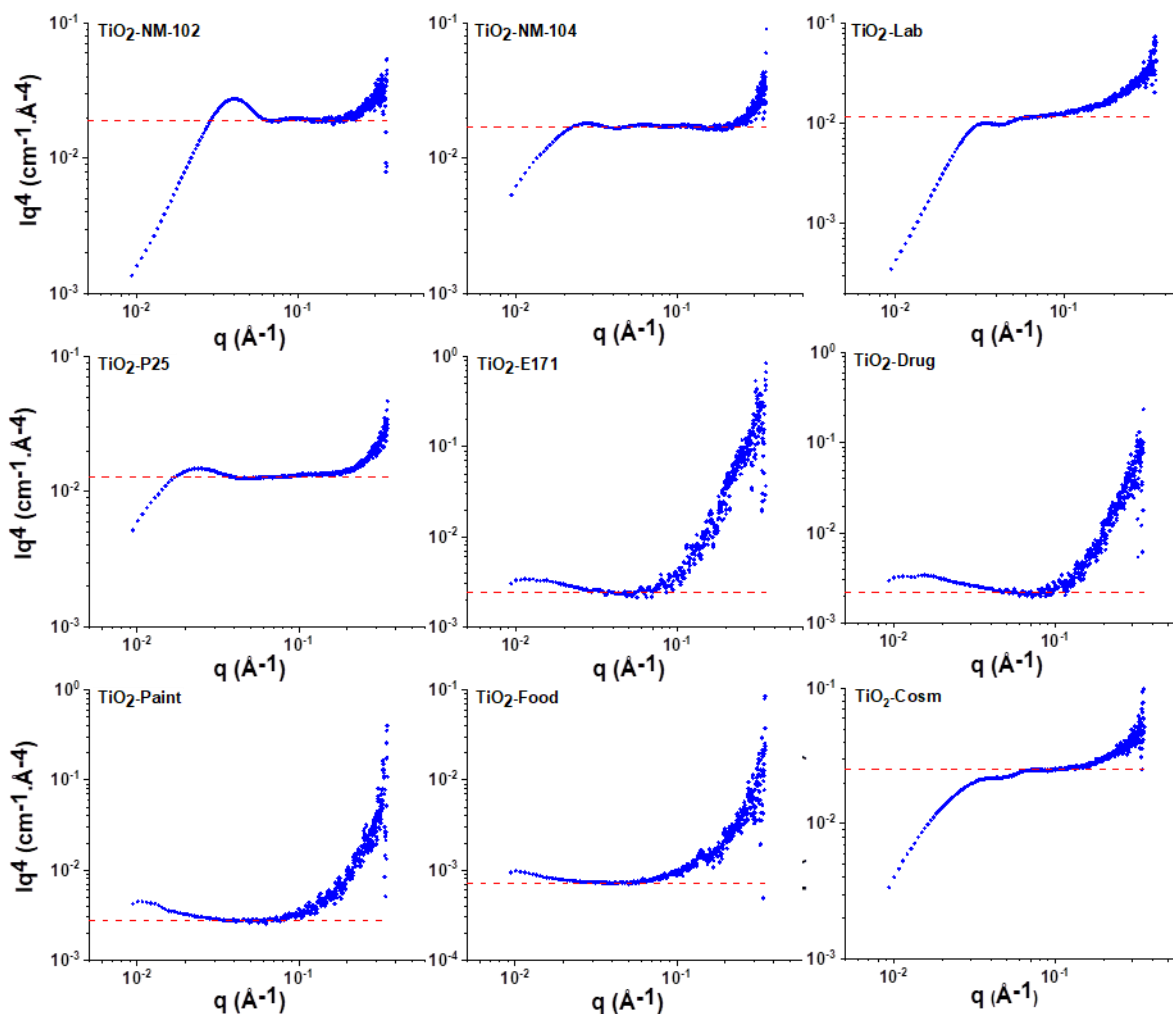


**Figure 4: Characteristic of TiO<sub>2</sub> nanoparticles in powder form by chemSAXS (after extraction from manufactured products), with a <10% transmission, in I(q)q<sup>4</sup> representations revealing Porod's Plateaus**

The intensities measured on the two set-up (chemSAXS - 8keV and MOMAC - 17keV) illustrate the extended q range for the Porod limit for the different samples and in particular (Figure S9) with a higher signal to noise ratio on an extended q range for the TiO<sub>2</sub>-E171, TiO<sub>2</sub>-Drug and TiO<sub>2</sub>-Paint. The SAXS measurements have been treated separately to compare the  $D_{Porod}$  eq (Figure 4 and Figure S10) and show a good agreement with each other's. For the following, only the measurements from chemSAXS are discussed.

For the analysis, the SLD (scattering length density) contrast between pure TiO<sub>2</sub> and air has been considered, with an SLD contrast value of  $3.18 \times 10^{11} \text{ cm}^{-2}$  and  $3.42 \times 10^{11} \text{ cm}^{-2}$  for anatase and

rutile phases respectively and  $3.22 \times 10^{11} \text{ cm}^{-2}$  for TiO<sub>2</sub>-P25 which contains a mixture of anatase (82%) and rutile (18%). This assumption is certainly not valid for the TiO<sub>2</sub>-Food sample. Chemical analyses have shown the presence of only 25% of TiO<sub>2</sub> in the sample and the existence of other element with probably a majority of residual wax. The intensity was normalized by considering this composition and the SLD contrast have been calculated between TiO<sub>2</sub> and wax ( $2.4 \cdot 10^{11} \text{ cm}^{-2}$ ) and results are presented as TiO<sub>2</sub>-Food\* in the Table 7. The chemSAXS instrument results are summarized in Table 7.

**Table 7: The average specific surfaces and average equivalent Porod diameters extracted from a different number of chemSAXS measurements on the 9 TiO<sub>2</sub> powders of interest. A typical transmission, thickness and Porod limit are reported for each sample. The number of measurements, added under coma for each was used to evaluate the repeatability uncertainties.**

Sample	Transmission (%)	Thickness (μm)	Porod's Limit (cm <sup>-1</sup> .Å <sup>-4</sup> )	Σ <sub>Porod SSA</sub> (m <sup>2</sup> /g) ± u <sub>R</sub> (number of measurements)	D <sub>Porod eq</sub> (nm) ± u <sub>R</sub>
TiO <sub>2</sub> -NM 102	1.0	104.9	0.018486	74.5 ±5.3 (13)	20.6 ±1.7
TiO <sub>2</sub> -NM 104	1.6	88.0	0.017353	56.0 ±6.2 (4)	25.6 ±2.9
TiO <sub>2</sub> -Lab	0.7	112.6	0.012343	49.6 ±4.9 (8)	31.1 ±3.3
TiO <sub>2</sub> -P25	7.2	59.5	0.013003	48.4 ±2.2 (4)	31.1 ±1.4
TiO <sub>2</sub> -E171	0.01	204.0	0.002531	10.3 ±1.3 (11)	151.1 ±18.8
TiO <sub>2</sub> -Drug	0.07	165.8	0.00227	9.1 ±0.2 (8)	167.0 ±4.0
TiO <sub>2</sub> -Paint	0.1	152.5	0.002837	9.0 ±0.1 (2)	156.9 ±2.4
TiO <sub>2</sub> -Food	1.3	100.1	0.000707	2.8 ±0.2 (4)	549.5 ±41.6
TiO <sub>2</sub> -Food(*)	1.3	100.1	0.000707	4.9 ±0.4 (4)	313.3 ±23.7
TiO <sub>2</sub> -Cosm	0.7	105.1	0.025079	81.2 ±3.7 (8)	17.5 ±0.7

*\*Treated by considering 25% of TiO<sub>2</sub> and 75% of WAX in the extracted powder*

As for the other techniques mentioned above, the two TiO<sub>2</sub> references NM102 and NM104 were analyzed by SAXS as part of the Nanogenotox Project [15]. In the JRC report, both samples particle sizes were extracted in two different ways; first via a unified model providing access to the gyration diameters of the primary particles and then by evaluating the total amount of interface between the two phases, i.e. air and TiO<sub>2</sub>, from which an equivalent Porod diameter is extracted. For comparison of the SAXS measurements, only Porod equivalent diameters are considered. For TiO<sub>2</sub>-NM102 and TiO<sub>2</sub>-NM104, D<sub>Porod eq</sub> of 20.6 nm (with a 74.5 m<sup>2</sup>/g specific surface area) and 25.6 nm (with a 56.0 m<sup>2</sup>/g specific surface area) are respectively obtained (Table 7). These results are in agreement with those published by the JRC for TiO<sub>2</sub>-NM-104 (52.4 ±2.1 m<sup>2</sup>/g corresponding to a diameter of 27 nm from JRC) but are slightly different for TiO<sub>2</sub>-NM102 with a 12% higher specific surface than the JRC mesurand (65.6 ± 3.3 m<sup>2</sup>/g corresponding to a diameter of 22 nm). This difference can be explained by

the fact that they used the same density ( $4.23 \text{ g}\cdot\text{cm}^{-3}$ ) and thus the same scattering length density (SLD) for all the samples whereas they are two different phases (anatase for  $\text{TiO}_2$ -NM102 and rutile for  $\text{TiO}_2$ -NM104). For both  $\text{TiO}_2$ -P25 ( $31.1 \pm 1.4 \text{ nm}$ ) and  $\text{TiO}_2$ -Lab ( $31.1 \pm 3.3 \text{ nm}$ ) samples, comparable  $D_{\text{Porod eq}}$  were found. For  $\text{TiO}_2$ -P25, this result is in agreement with the  $29.6 \text{ nm}$  diameter measured from the Guinier law approach by Guo et al. [73].

The chemSAXS results for the additive  $\text{TiO}_2$ -E171 and the extracted particles  $\text{TiO}_2$ -Drug and  $\text{TiO}_2$ -Paint show close  $D_{\text{Porod eq}}$  values ( $151.1 \pm 18.8 \text{ nm}$ ,  $167.0 \pm 4.0 \text{ nm}$  and  $156.9 \pm 2.4 \text{ nm}$ , respectively). On the contrary, a much higher  $D_{\text{Porod eq}}$  was measured for the  $\text{TiO}_2$ -Food, while SEM images have shown that these sample particles are similar to the three previous ones (Figure 2). This discrepancy can come from the low content of  $\text{TiO}_2$  in the extracted powder from  $\text{TiO}_2$ -Food which induces a strong bias in the SAXS analysis. The  $D_{\text{Porod eq}}$  value considering the wax proportion (at 75%) is lower ( $313.3 \pm 23.7 \text{ nm}$ ) than the first value ( $549.5 \pm 41.6 \text{ nm}$ ) but still far from those of samples with similar particles (i.e.  $\text{TiO}_2$ -E171,  $\text{TiO}_2$ -Drug and  $\text{TiO}_2$ -Paint). We only consider wax for data treatment, however other impurities are identified in this sample according to ICP-OES and XPS measurements.

For the anisotropic sample,  $\text{TiO}_2$ -Cosm, a  $17.1 \pm 0.7 \text{ nm}$   $D_{\text{Porod eq}}$  was obtained, showing that this extracted material contain  $\text{TiO}_2$  particles smaller than the others. This is a first indication of different  $\text{TiO}_2$  types embedded in the manufactured products. For the references, synthesized, pristine and extracted  $\text{TiO}_2$  materials, the Porod limit approach permits comparing the specific surface and the equivalent Porod diameter on a large size range.

## 4. Discussion

### 4.1 Comparison between specific surface area obtained by SAXS and BET

BET technique is considered as the reference method [20] and is widely used to reach in a reproducible way the specific surface area for material in powder form [57], with a similar measurand given by SAXS. Figure 5 gives an overview of the specific surfaces areas measured by BET and SAXS (BET isotherms are illustrated in the Figure S7). In this work, a relation between the specific surface area obtained by SAXS and BET, have been illustrated (Figure 5) on a set of raw  $\text{TiO}_2$ -particles and extracted  $\text{TiO}_2$ -particles from commercial products. In the JRC report similar data were obtained for the BET measurements regarding  $\text{TiO}_2$ -NM102 and  $\text{TiO}_2$ -NM-104 [15]. The BET results achieved for  $\text{TiO}_2$ -P25 and additive  $\text{TiO}_2$ -E171 are in compliance with those published in previous work [39,64,74]. Concerning extracted NPs, the  $\text{TiO}_2$ -Food and  $\text{TiO}_2$ -Drug could not be measured by BET because of their too low amount of  $\text{TiO}_2$  extracted in powder form. Only, SAXS measurements have been

performed on these two samples. Regarding specific surface area measurements, different families of compounds can be classified. The highest specific surface ( $\sim 80 \text{ m}^2/\text{g}$ ) is found for  $\text{TiO}_2\text{-NM102}$  and  $\text{TiO}_2\text{-Cosm}$ , then  $\text{TiO}_2\text{-NM104}$ ,  $\text{TiO}_2\text{-Lab}$  and  $\text{TiO}_2\text{-P25}$  have a specific surface area around  $50 \text{ m}^2/\text{g}$  and finally  $\text{TiO}_2\text{-E171}$ ,  $\text{TiO}_2\text{-Paint}$  and  $\text{TiO}_2\text{-Drug}$  have the lowest value around  $10 \text{ m}^2/\text{g}$ . All details are presented in the Table S6.

Specific surface area with Porod's law indicates a similar value between  $\text{TiO}_2\text{-Drug}$  and  $\text{TiO}_2\text{-Paint}$ , excepted for  $\text{TiO}_2\text{-Food}$ , that dealing with the same family of  $\text{TiO}_2$  pigments.

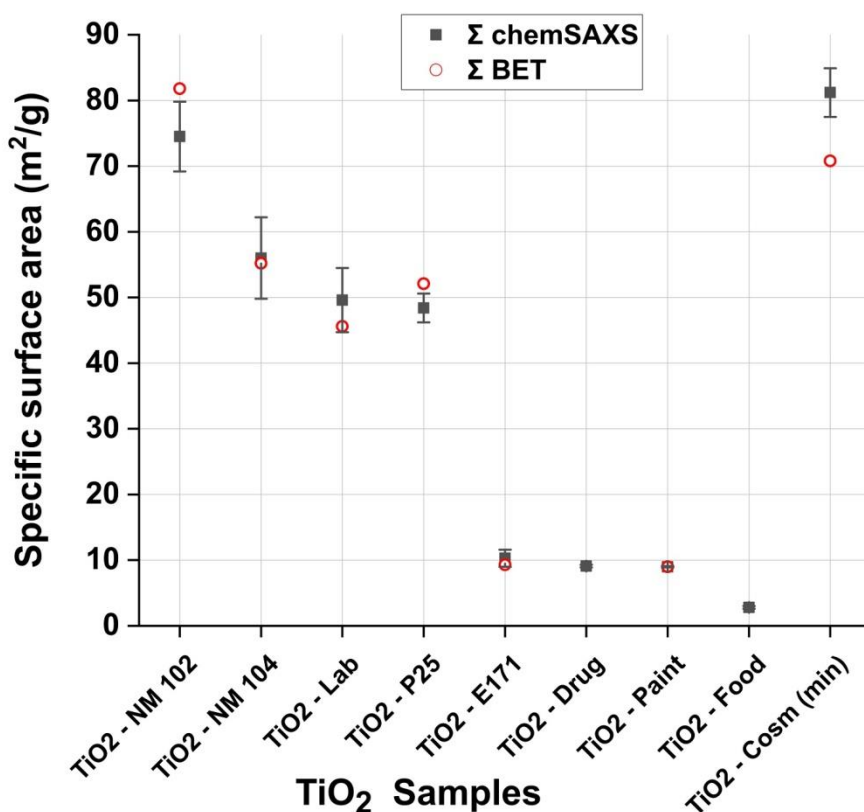


Figure 5 :  $\text{TiO}_2$ -samples BET and SAXS surface specific area

For most investigated samples, no significant discrepancies to within uncertainties are observed between the specific surface obtained by SAXS and the BET, which does not come unexpectedly for non-porous and near-spherical particles. Based on a specific surface area comparison, a good agreement is obtained between BET and SAXS for all  $\text{TiO}_2$ -particles excepted for extracted  $\text{TiO}_2\text{-cosm}$  with 13% of differences.

The specific surface measured by both methods, SAXS and BET, are suitable to assess average size of raw nanomaterials and extracted particles, but is not suitable to determine the content of nanoparticles and size distribution.

## 4.2 Comparison of SAXS and SEM equivalent diameters

For particles characterization dimensional measurement are usually required to define nanosize. An equivalent diameter (assuming a particles spherical shape) was calculated from Porod SAXS datas and compared to geometrical diameter measured by SEM. All the results are reported in Table 8.

**Table 8 : Equivalent diameter of TiO<sub>2</sub> samples measured by SAXS, SEM and relative discrepancies associated**

Sample	SAXS	SEM	Relative discrepancy deviation
	D <sub>eq Porod</sub> ±u <sub>R</sub> (nm)	D <sub>SEM Average area-eq</sub> ±u <sub>R</sub> (nm)	U <sub>d</sub> (%)
TiO <sub>2</sub> -NM 102	<b>20.6 ± 1.7</b>	<b>26.8 ± 3.1</b>	<b>22</b>
TiO <sub>2</sub> -NM 104	<b>25.6 ± 2.9</b>	<b>27.3 ± 0.5</b>	<b>6</b>
TiO <sub>2</sub> -Lab	<b>31.1 ± 3.3</b>	<b>21.1 ± 0.9</b>	<b>48</b>
TiO <sub>2</sub> -P25	<b>31.1 ± 1.4</b>	<b>25.8 ± 1.2</b>	<b>20</b>
TiO <sub>2</sub> -E171	<b>151.1 ± 18.8</b>	<b>110.2 ± 4.4</b>	<b>37</b>
TiO <sub>2</sub> -Drug	<b>167.0 ± 4.0</b>	<b>128.4 ± 2.1</b>	<b>30</b>
TiO <sub>2</sub> -Paint	<b>156.9 ± 2.4</b>	<b>146.6 ± 2.5</b>	<b>7</b>
TiO <sub>2</sub> -Food	<b>549.5 ± 41.6</b>	<b>133.2 ± 3.9</b>	<b>313</b>
TiO <sub>2</sub> -Cosm		<b>27.9 ± 0.9</b>	<b>37</b>
TiO <sub>2</sub> -Cosm (Feret max and min)	<b>17.5 ± 0.7</b>	<b>D<sub>Fmax</sub> = 51.9 ± 1.0</b> <b>D<sub>Fmin</sub> = 15.8 ± 2.8</b>	<b>*</b>

\*Not calculated

When shifting from specific surface to an equivalent diameter, there is a significant difference between SEM and SAXS results in some cases. For TiO<sub>2</sub>-NM104, the two equivalent diameters are similar as observed in the JRC report [15] while a slight divergence is observed for the TiO<sub>2</sub>-NM102 (~20 % of relative discrepancy). In JRC report it was mentioned the difficulty to measure NM102 due to dispersion problem. A similar divergence is also observed for TiO<sub>2</sub>-P25 sample (31.1 ± 1.4 nm and 25.8 ± 1.2 nm for SAXS and SEM results respectively). In the same way, the synthesized sample, TiO<sub>2</sub>-Lab, has a D<sub>SEM average area-eq</sub> equal to 21.1 ± 0.9 nm, a slightly lower value than that provided by SAXS (31.1 ± 3.3 nm). For both TiO<sub>2</sub>-P25 and TiO<sub>2</sub>-Lab samples, the polydispersity in shape, the high state of agglomeration, and the particles small size (clearly observed on SEM images in Figure 2) can negatively impact the SEM measurement accuracy and could influence the equivalent diameter determination with a sphere assumption from Porod SAXS data.

For the additive TiO<sub>2</sub>-E171, the size distribution is quite wide (50-300 nm with a size distribution standard deviation of 37.2 ± 2.2 nm) which means this studied sample is highly polydispersed in size. Indeed, the SAXS D<sub>Porod eq</sub> value measured (151.1 ± 18.8 nm) is, higher than that obtained by electron

microscopy ( $110.2 \pm 4.4$  nm). These findings were similar for the extracted samples (TiO<sub>2</sub>-Drug, TiO<sub>2</sub>-Paint, and TiO<sub>2</sub>-Food) with a SAXS  $D_{\text{Porod eq}}$  higher than the  $D_{\text{SEM average area-eq}}$  measured by SEM (Table 8). As for the additive TiO<sub>2</sub>-E171, these three samples are polydisperse in size.

Significant differences are observed for TiO<sub>2</sub>-Food sample. The SAXS  $D_{\text{Porod eq}}$  is 4 times larger than the  $D_{\text{SEM average area-eq}}$ . As explained above, this discrepancy could come from impurities present in this sample or from the polydispersity in size. Indeed, plates of matrix residues were observed through SEM-EDS analysis, which may be the source of the larger gap noted between the two techniques results. In fact, the presence of other elements than TiO<sub>2</sub> can influence both the measurement (presence of a compound that promotes strong interactions between particles) and the data processing (sample purity assumption for transmission calculation and specific surface extraction from Porod limit).

The TiO<sub>2</sub>-Cosm sample presents a SAXS  $D_{\text{Porod eq}}$  very similar to  $D_{\text{SEM average Fmin}}$  assessed by SEM with an equivalent diameter of  $17.5 \pm 0.7$  nm for the SAXS and  $15.8 \pm 2.8$  nm for the SEM.

To conclude on the SAXS/SEM measurements, a discrepancy is observed between  $D_{\text{Porod eq}}$  and  $D_{\text{SEM average area-eq}}$ . Only the two reference samples TiO<sub>2</sub>-NM102 and TiO<sub>2</sub>-NM104 show smaller  $D_{\text{Porod eq}}$  than the  $D_{\text{SEM average area-eq}}$ . Yet, for the most of TiO<sub>2</sub> samples, the SAXS  $D_{\text{Porod eq}}$  is larger than the  $D_{\text{SEM average area-eq}}$  with deviations ranging from 6% (TiO<sub>2</sub>-NM104) to 48% (TiO<sub>2</sub>-Lab), excluding the TiO<sub>2</sub>-Food. These results show the difficulty in measuring and comparing (nano) particles size from different techniques. This point has been largely supported by intercomparison studies [1,75] and has been related to the nanoparticles polydispersity in size and to the difficulties in extracting the particles and preparing the samples. In addition the different measurands nature given by SEM (projected surface) and SAXS (specific surface area) and the extracted equivalent diameter assuming spherical particles, increase the comparison complexity [76].

### **4.3 Influence of polydispersity on SAXS and SEM equivalent diameters**

When comparing the SAXS and SEM equivalent diameters, differences were observed (Figure 6). It appears that the average diameter used to compare these two measurands should be discussed to take into account the samples size polydispersity. Deschamp et al. [77] have shown the strong polydispersity influence on the Porod radius. Assuming a spheres lognormal distribution, the experimental Porod radius corresponds to a sphere radius of an equivalent surface to volume ratio measured by the distribution. It should be compared to the values resulting from the distribution (when the distribution is known) (Equation 6)).

$$R_{Porod Eq calc} = 3 \frac{V}{S} = 3 \frac{\int f(R)R^3 dR}{\int f(R)R^2 dR} = \frac{D_{Porod Eq calc}}{2} \quad \text{Equation 6}$$

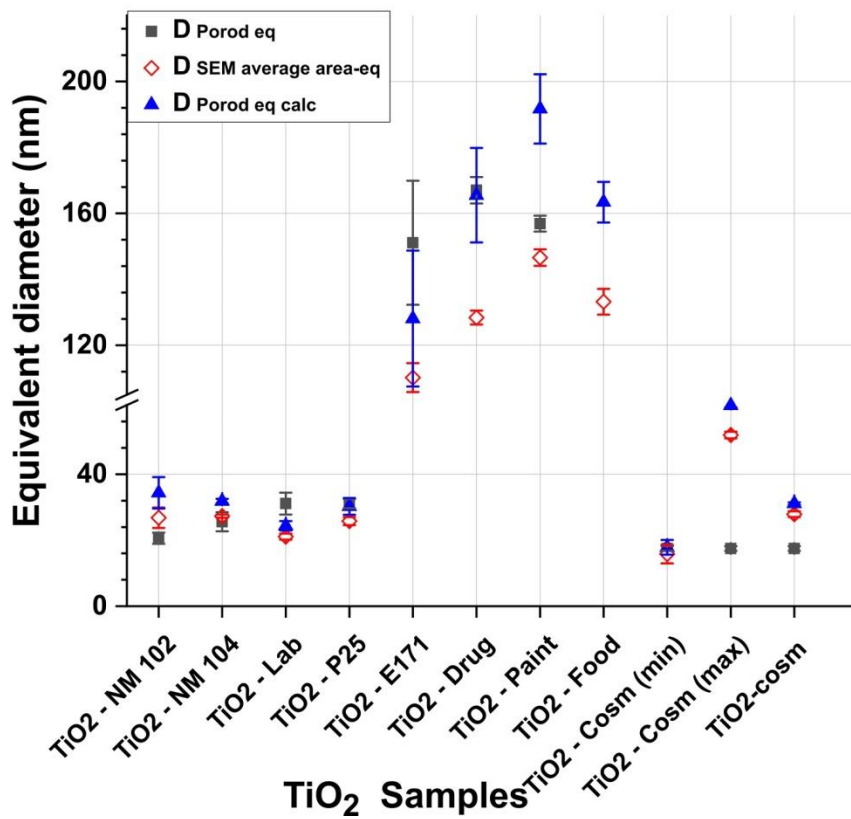


Figure 6 : TiO<sub>2</sub>-samples, SEM and Porod's (measured and calculated) equivalent diameters

Deschamp et al. [77] have shown that for a lognormal distribution with increasing the standard deviation, the Porod radius (calculated or experimental) differs from the lognormal distribution median radius and from the Guinier radius (obtained at low  $q$  range). Figure S11 shows the variation of the  $D_{Porod Eq calc}$  with increasing the standard deviation of the distribution. The difference between  $D_{Porod Eq calc}$  and  $D_{SEM Average area-eq}$  is more and more important with increasing the expansion of the distribution.

**Table 9: Comparison between the SEM mean equivalent diameter, the equivalent Porod diameter calculated with the SEM size distribution of TiO<sub>2</sub> particles and the SAXS equivalent diameter determined from the Porod's limit ( $u_R$  is the repeatability uncertainty)**

Sample	$D_{SEM\ Average\ area-eq}$ (nm) $\pm u_R$	Standard deviation of the SEM size distribution $\pm u_R$	$D_{Porod\ eq\ calc}$ calculated with Lognormal distribution (nm) $\pm u_R$	$D_{Porod\ eq}$ determined from Porod's limit (nm) $\pm u_R$	Aspect Ratio
TiO <sub>2</sub> -NM102	26.8 $\pm$ 3.1	9.7 $\pm$ 1.7	34.4 $\pm$ 4.8	20.6 $\pm$ 1.7	0.7
TiO <sub>2</sub> -NM104	27.3 $\pm$ 0.5	7.7 $\pm$ 0.8	31.8 $\pm$ 0.7	25.6 $\pm$ 2.9	0.7
TiO <sub>2</sub> -Lab	21.1 $\pm$ 0.9	5.8 $\pm$ 0.6	24.4 $\pm$ 1.4	31.1 $\pm$ 3.3	0.8
TiO <sub>2</sub> -P25	25.8 $\pm$ 1.2	7.4 $\pm$ 1.4	30.3 $\pm$ 2.5	31.1 $\pm$ 1.4	0.9
TiO <sub>2</sub> -E171	110.2 $\pm$ 4.4	37.2 $\pm$ 2.2	128.1 $\pm$ 20.6	151.1 $\pm$ 18.8	0.8
TiO <sub>2</sub> -Drug	128.4 $\pm$ 2.1	46.8 $\pm$ 7.7	165.5 $\pm$ 14.3	167.0 $\pm$ 4.0	0.9
TiO <sub>2</sub> -Paint	146.6 $\pm$ 2.5	55.3 $\pm$ 5.9	191.7 $\pm$ 10.5	156.9 $\pm$ 2.4	0.8
TiO <sub>2</sub> -Food	133.2 $\pm$ 3.9	43.6 $\pm$ 2.6	163.4 $\pm$ 6.2	549.5 $\pm$ 41.6	0.9
TiO <sub>2</sub> -Cosm	27.9 $\pm$ 0.9	6.6 $\pm$ 0.4	31.1 $\pm$ 0.4		
TiO <sub>2</sub> -Cosm (F <sub>max</sub> )	51.9 $\pm$ 1.0	14.9 $\pm$ 0.4	60.9 $\pm$ 0.6	17.5 $\pm$ 0.7	0.3
TiO <sub>2</sub> -Cosm (F <sub>min</sub> )	15.8 $\pm$ 2.8	3.9 $\pm$ 0.1	17.8 $\pm$ 2.2		

The  $D_{Porod\ Eq\ calc}$  is the average value issued from the calculation of Porod diameter for the three SEM lognormal distributions obtained for each TiO<sub>2</sub>-sample (Equation 6). For a lognormal distribution of spheres, the calculated value should be equal to the experimental one. For the particles with a quasi-spherical shape (TiO<sub>2</sub>-P25 and TiO<sub>2</sub>-Drug), the  $D_{Porod\ Eq\ calc}$  is similar to the measured  $D_{Porod\ eq}$  while differences are increasing between the two values when particles strongly deviates from sphericity (i.e with an aspect ratio inferior or equal to 0.8). The Figure 6 indicates that the  $D_{Porod\ Eq\ calc}$  are systematically larger than the average  $D_{SEM\ Average\ area-eq}$ . Indeed, the larger the standard deviation of the size distribution (Table 9), the greater the difference between the two equivalent diameters. As previously mentioned, the  $D_{eq\ Porod}$  are very close for the TiO<sub>2</sub>-E171 and the two samples extracted from TiO<sub>2</sub>-Drug and TiO<sub>2</sub>-Paint products. These similarities are not observed for  $D_{Porod\ Eq\ calc}$  calculated from distribution issued from SEM where the diameter ( $D_{SEM\ Average\ area-eq}$ ) are different.  $D_{Porod\ eq}$  measured for the TiO<sub>2</sub>-Food is not represented in the Figure 6 because this value is considered an outlier.

The case of TiO<sub>2</sub>-Cosm is distinct because these particles are strongly anisotropic.  $D_{Porod\ Eq\ calc}$  calculated from the distributed diameters assuming a spherical shape is larger (31.1  $\pm$  0.4 nm) than the SAXS measured value (17.5  $\pm$  0.7 nm) but close to the  $D_{SEM\ Average\ area-eq}$  obtained by considering spherical particles.

Taking size polydispersity into account does not explain all the discrepancies between equivalent diameter extracted from SAXS and SEM measurands. It appears that the spherical hypothesis used for the description of the SEM size distribution and for the diameter determination from Porod limit is a strong limitation. The aspect ratio and the large lognormal size distribution contribute to the difficulties in comparing different measurands.

#### 4.4 Impact of interaction between particles on equivalent diameter measurements

The interaction between particles can lead to agglomeration or aggregation steps. The (nano) particles can be isolated or in the form of agglomerates and/or aggregates. The EC recommendation makes a difference between these two structures [4]. Indeed, in the case of agglomerates, the particles bind to each other through weak bonds (as the Van-der-Waals or electrostatic forces) while being tangential to one another. In contrast with agglomerates, aggregates are made of nano-objects strongly linked together (covalent bonds) and are difficult to separate, since this phenomenon is irreversible (partial fusion).

The values from  $D_{\text{Porod eq}}$  (or  $D_{\text{eq BET}}$ ) and  $D_{\text{SEM Average area-eq}}$  for the nine TiO<sub>2</sub> powders studied are presented in Table 10 which highlights divergences between the two methods (SAXS or BET) and SEM measurements. The specific surface area obtained by SAXS or BET method for some samples (TiO<sub>2</sub>-Lab, TiO<sub>2</sub>-E171, TiO<sub>2</sub>-Drug, TiO<sub>2</sub>-Paint and TiO<sub>2</sub>-Food) presents a too low value compared to that expected from the  $D_{\text{SEM average area-eq}}$  values. Thus, the equivalent diameters obtained for these samples, by integral methods reported in Table 10, are systematically higher than  $D_{\text{SEM Average area-eq}}$ . In addition, for TiO<sub>2</sub>-Cosm, the specific surface give a diameter ( $D_{\text{Porod eq}}$ ) in agreement with the smallest dimension of the particles ( $D_{\text{Fmin}}$ ). This indicate a higher contribution of the small size of the particles in the specific surface measurement which could be related to an agglomerate of the particles along their longest dimension.

**Table 10 : Equivalent diameter of TiO<sub>2</sub> samples measured by SAXS and BET versus SEM**

Sample	SAXS	BET*	SEM
	D <sub>Porod eq</sub> ± u <sub>R</sub> (nm)	D <sub>eq BET</sub> (nm)	D <sub>SEM Average area-eq</sub> ± u <sub>R</sub> (nm)
TiO <sub>2</sub> -NM 102	20.6 ± 1.7	18.7	26.8 ± 3.1
TiO <sub>2</sub> -NM 104	25.6 ± 2.9	25.7	27.3 ± 0.5
TiO <sub>2</sub> -Lab	31.1 ± 3.3	33.5	21.1 ± 0.9
TiO <sub>2</sub> -P25	31.1 ± 1.4	28.8	25.8 ± 1.2
TiO <sub>2</sub> -E171	151.1 ± 18.8	164.3	110.2 ± 4.4
TiO <sub>2</sub> -Drug	167.0 ± 4.0	-	128.4 ± 2.1
TiO <sub>2</sub> -Paint	156.9 ± 2.4	157.4	146.6 ± 2.5
TiO <sub>2</sub> -Food	549.5 ± 41.6	-	133.2 ± 3.9
TiO <sub>2</sub> -Cosm			27.9 ± 0.9
TiO <sub>2</sub> -Cosm (Feret min et max)	17.5 ± 0.7	20.1 (spherical hypothesis) 13.4 (elongated hypothesis)	D <sub>Fmax</sub> = 51.9 ± 1.0 D <sub>Fmin</sub> = 15.8 ± 2.8

\*Equivalent diameter for TiO<sub>2</sub>-Drug and TiO<sub>2</sub>-Food can be not calculated for BET. For TiO<sub>2</sub>-Cosm, the values for either the isotropic shape hypothesis or the elongated shape hypothesis are given (see Table S6).

The SEM does not appear to be able to distinguish between strong and weak bonds. Indeed, the particles are measured taking into account the constituent particles and thus measuring NPs within aggregates/agglomerates. For all TiO<sub>2</sub>-samples, D<sub>SEM average area-eq</sub> presents the average size of primary particles obtained from number-based size distributions. The overlap of primary particles should be taken into account in the all cases. Defined as integral techniques, the BET and SAXS analyze all particles (constituents and agglomerated/aggregates forms) measuring the total specific surface, and not the size distribution. In fact, on the one hand we have an overall methods (10<sup>10</sup> particles measured) representative of the studied sample, while on the other hand we have a direct and local method which provides us an access to the shape and the smallest particle dimension (required by the regulation) but where only 300 particles are counted without distinguishing agglomerates from aggregates. This translates into an important deviation in terms of equivalent diameter compared to the SEM and thus demonstrates the presence of strong interactions and aggregates.

## 5. Conclusion

The aim of this study was to compare the dimensional analysis of TiO<sub>2</sub>-particles from an indirect method (SAXS) with diameter (D<sub>Porod eq</sub>) extracted from the specific surface mesurand and a direct method (SEM) with the diameter equivalent to a projected surface area (D<sub>SEM Average area-eq</sub>). Despite the hypotheses (composition and size polydispersity), the two techniques comparison results show relative discrepancies between D<sub>Porod eq</sub> and the D<sub>SEM Average area-eq</sub>. Polydispersity in size doesn't explain all variation and the interaction between particles and form complexity seems to be the most influent contributors through specific surface area considerations, leading to a final SAXS equivalent diameters always larger than the SEM ones. We have shown that from surface specific particles, the hypothesis

on the spherical shape for diameter extraction is too limited to account to a real shape of the particles. In addition, the presence of aggregates in the powder influences strongly the specific surface measurement by integral techniques. The different techniques families such as SEM and SAXS are complementary depending on the type of dimensional characterization required.

This article deals only with TiO<sub>2</sub>-particles in powder form. Results underlines that the measurements of dimensional (nano)particles in complex media need an extraction steps that is a critical point for the analysis. In particular for global analysis such as SAXS, where impurities can interact with particles of interest. Beyond this crucial point, there is a real need for direct analysis of NPs in complex media. In situ measurement by SAXS, in a colloidal suspension remains an issue to be studied and evaluated.

## 6. Sample Credit author statement

**Najoua Bouzakher-Ghomrasni:** Investigation, Formal analysis, Draft preparation, writing **Olivier Tache:** SAXS acquisition, software, Formal analysis, Conceptualization **Jocelyne Leroy:** XPS analysis, **Nicolas Feltin:** Writing, Review and editing, Conceptualization **Fabienne Testard:** Supervision, Conceptualization, Formal analysis, validation, writing -review&editing **Carine Chivas-Joly:** Supervision, Conceptualization, Formal analysis, validation, writing -review&editing.

## 7. Acknowledgements

The authors want to thanks J-F Hochepped for his help on the synthesis protocol for TiO<sub>2</sub>-lab. The authors acknowledge the financial support from Agence Nationale Recherche Technologie (ANRT) under the contract CIFRE N°2018/0367.

### References

- [1] F. Babick, J. Mielke, W. Wohlleben, S. Weigel, V.D. Hodoroaba, How reliably can a material be classified as a nanomaterial? Available particle-sizing techniques at work, *J. Nanoparticle Res.* 18 (2016) 1–40. doi:10.1007/s11051-016-3461-7.
- [2] ISO/TF 13014:2012, Nanotechnologies – Guidance on Physico-chemical Assessment, Characterization of Engineered Nanoscale Materials for Toxicologic, 2012.
- [3] ISO/TS 80004-1:2015, Nanotechnologies — Vocabulaire — Partie 1: Termes “coeur,” 2015. <https://www.iso.org/obp/ui/#iso:std:iso:ts:80004:-1:ed-2:v1:fr>.
- [4] European commission, Recommendation on the definition of nanomaterial, Off. J. Eur. Union.

- (2011). [http://ec.europa.eu/health/scientific\\_committees/emerging/docs/](http://ec.europa.eu/health/scientific_committees/emerging/docs/).
- [5] European Commission, Regulation (EC) No 1223/2009 of the European Parliament and of the Council on cosmetic products, *Off. J. Eur. Union*. (2016).
- [6] European Council Regulations, Regulation (EU) 2015/2283 on novel foods, *Off. J. Eur. Union*. 327 (2015) 1–22.
- [7] European Commission, Regulation (EU) No 528/2012 of the European Parliament and of the Council of 22 concerning the making available on the market and use of biocidal product, *Off. J. Eur. Union*. (2012) 1–123. doi:10.5040/9781782258674.0009.
- [8] French nanomaterials register website [www.r-nano.fr](http://www.r-nano.fr), (n.d.). <https://www.r-nano.fr/> (accessed March 1, 2021).
- [9] European Commission, Regulation (EU) 2018/1881 of 3 December 2018 amending Regulation (EC) No 1907/2006 of the European Parliament and of the Council on the Registration, Evaluation, Authorisation and Restriction of Chemicals (REACH) as regards Annexes I, III, VI, V, *Off. J. Eur. Union*. (2018).
- [10] EFSA, Guidance on the risk assessment of the application of nanoscience and nanotechnologies in the food and feed chain, *EFSA J.* 9 (2011) 1–36. doi:10.2903/j.efsa.2011.2140.
- [11] C. Contado, Nanomaterials in consumer products: A challenging analytical problem, *Front. Chem.* 3 (2015) 1–20. doi:10.3389/fchem.2015.00048.
- [12] F. Varenne, L. Devoille, A. Makky, N. Feltin, F. Violleau, G. Barratt, C. Vauthier, Evaluation of the size distribution of a multimodal dispersion of polymer nanoparticles by microscopy after different methods of deposition, *J. Drug Deliv. Sci. Technol.* 60 (2020) 1–11. doi:10.1016/j.jddst.2020.102047.
- [13] C. Guiot, O. Spalla, Stabilization of TiO<sub>2</sub> Nanoparticles in Complex Medium through a pH Adjustment Protocol, *Environ. Sci. Technol.* 47 (2013) 1057–1064. doi:10.1021/es3040736.
- [14] V. Geertsen, E. Barruet, F. Gobeaux, J.L. Lacour, O. Taché, Contribution to Accurate Spherical Gold Nanoparticle Size Determination by Single-Particle Inductively Coupled Mass Spectrometry: A Comparison with Small-Angle X-ray Scattering, *Anal. Chem.* 90 (2018) 9742–9750. doi:10.1021/acs.analchem.8b01167.
- [15] K. Rasmussen, J. Mast, P.-J. De Temmerman, E. Verleysen, N. Waegeneers, F. Van Steen, J.C. Pizzolon, L. De Temmerman, E. Van Doren, K.A. Jensen, R. Birkedal, M. Levin, S.H. Nielsen, I.K. Koponen, P.A. Clausen, V. Kofoed-Sørensen, Y. Kembouche, N. Thieriet, O. Spalla, C. Guiot, D. Rousset, O. Witschger, S. Bau, B. Bianchi, C. Motzkus, B. Shivachev, L. Dimowa, R. Nikolova, D. Nihtianova, M. Tarassov, O. Petrov, S. Bakardjieva, D. Gilliland, F. Pianella, G. Ceccone, V. Spampinato, G. Cotogno, N. Gibson, C. Gaillard, A. Mech, Titanium Dioxide, NM-100, NM-101, NM-102, NM-103, NM-104, NM-105: Characterisation and Physico- Chemical Properties, 2014. doi:10.2788/79554.
- [16] Z.H. Chen, C. Kim, X.B. Zeng, S.H. Hwang, J. Jang, G. Ungar, Characterizing size and porosity of hollow nanoparticles: SAXS, SANS, TEM, DLS, and adsorption isotherms compared, *Langmuir*. 28 (2012) 15350–15361. doi:10.1021/la302236u.
- [17] S. Pabisch, B. Feichtenschlager, G. Kickelbick, H. Peterlik, Effect of interparticle interactions on size determination of zirconia and silica based systems - A comparison of SAXS, DLS, BET,

- XRD and TEM, Chem. Phys. Lett. 521 (2012) 91–97. doi:10.1016/j.cplett.2011.11.049.
- [18] H. Jensen, J.H. Pedersen, J.E. Jorgensen, J.S. Pedersen, K.D. Joensen, S.B. Iversen, E.G. Sogaard, Determination of size distributions in nanosized powders by TEM, XRD, and SAXS, J. Exp. Nanosci. 1 (2006) 355–373. doi:10.1080/17458080600752482.
- [19] B.R. Pauw, C. Kästner, A.F. Thünemann, Nanoparticle size distribution quantification: Results of a small-angle X-ray scattering inter-laboratory comparison, J. Appl. Crystallogr. 50 (2017) 1280–1288. doi:10.1107/S160057671701010X.
- [20] V.-D. Hodoroaba, J. Mielke, Techniques evaluation report for selection of characterisation methods The NanoDefine Consortium 2015 (www.nanodefine.eu), 2015.
- [21] W. Wohlleben, J. Mielke, V.-D. Hodoroaba, A. Zimathies, A. Bianchin, A. Lecloux, G. Roebben, H. Rauscher, N. Gibson, Development of an integrated approach based on validated and standardized methods to support the implementation of the EC recommendation for a definition of nanomaterial, J. Nanoparticle Res. 19 (2017). doi:10.1007/s11051-017-3741-x.
- [22] H. Rauscher, A. Mech, V. Kestens, R. Koeber, T.P.J. Linsinger, E.A. Stefaniak, Identification of nanomaterials through measurements (JRC science for policy report), 2019. doi:10.2760/053982.
- [23] X. Chen, A. Selloni, Introduction: Titanium Dioxide (TiO<sub>2</sub>) Nanomaterials, Chem. Rev. 114 (2014) 9281–9282. doi:10.1021/cr500422r.
- [24] A.J. Haider, Z.N. Jameel, I.H.M. Al-Hussaini, Review on: Titanium dioxide applications, Energy Procedia. 157 (2019) 17–29. doi:10.1016/j.egypro.2018.11.159.
- [25] General Directorate of Risk Prevention, Study report on the elements resulting from the declarations of substances in the nanoparticle state for 2019, 2020. <https://www.ecologie.gouv.fr/sites/default/files/Rapport R-nano 2019.pdf>.
- [26] French Government Decree - Order of 17 Avril 2019 suspending the placing on the market of food stuffs containing the additive E 171 (titanium dioxide - TiO<sub>2</sub>), J. Off. La République Française. (2019). [https://www.legifrance.gouv.fr/download/pdf?id=5Ma2PrHxnC95\\_gRa\\_x-vmNTTi3CWu\\_4E7Em7OkjkFM=](https://www.legifrance.gouv.fr/download/pdf?id=5Ma2PrHxnC95_gRa_x-vmNTTi3CWu_4E7Em7OkjkFM=).
- [27] French Government Decree - Order of 21 December 2020 suspending the placing on the market of foodstuffs containing the additive E 171 (titanium dioxide - TiO<sub>2</sub>), J. Off. La République Française. (2020). <https://www.legifrance.gouv.fr/jorf/id/JORFTEXT000042739505>.
- [28] ANSES, Notice of the National Agency for Food, Environmental and Occupational Health Safety on nanomaterials in food products, 2020.
- [29] M. Younes, G. Aquilina, L. Castle, K.H. Engel, P. Fowler, M.J. Frutos Fernandez, R. Gürtler, U. Gundert-Remy, T. Husøy, W. Mennes, P.M. Agneta Oskarsson, S. Rainieri, R. Shah, I. Waalkens-Berendsen, D. Wölfle, E. Gaffet, J. Mast, R. Peters, A.M. Rincon, P. Fürst, Scientific opinion on the proposed amendment of the EU specifications for titanium dioxide (E 171) with respect to the inclusion of additional parameters related to its particle size distribution, EFSA J. 17 (2019) 1–23. doi:10.2903/j.efsa.2019.5760.
- [30] E. Verleysen, N. Waegeneers, F. Brassinne, S. De Vos, I.O. Jimenez, S. Mathioudaki, J. Mast, Physicochemical characterization of the pristine E171 food additive by standardized and validated methods, Nanomaterials. 10 (2020) 1–22. doi:10.3390/nano10030592.

- [31] The Nanodatabase ([www.nanodb.dk](http://www.nanodb.dk)) developed by the Danish Consumer Council, The Ecological council and DTU Environment, (2021).
- [32] N.B. Ghomrasni, C. Chivas-Joly, L. Devoille, J.F. Hochepped, N. Feltin, Challenges in sample preparation for measuring nanoparticles size by scanning electron microscopy from suspensions, powder form and complex media, *Powder Technol.* 359 (2020) 226–237. doi:10.1016/j.powtec.2019.10.022.
- [33] I. de la Calle, M. Menta, M. Klein, B. Maxit, F. Séby, Towards routine analysis of TiO<sub>2</sub> (nano)particle size in consumer products: Evaluation of potential techniques, *Spectrochim. Acta - Part B At. Spectrosc.* 147 (2018) 28–42. doi:10.1016/j.sab.2018.05.012.
- [34] I. de la Calle, M. Menta, M. Klein, F. Séby, Screening of TiO<sub>2</sub> and Au nanoparticles in cosmetics and determination of elemental impurities by multiple techniques (DLS, SP-ICP-MS, ICP-MS and ICP-OES), *Talanta.* 171 (2017) 291–306. doi:10.1016/j.talanta.2017.05.002.
- [35] I. de la Calle, M. Menta, M. Klein, F. Séby, Study of the presence of micro- and nanoparticles in drinks and foods by multiple analytical techniques, *Food Chem.* 266 (2018) 133–145. doi:10.1016/j.foodchem.2018.05.107.
- [36] A. Philippe, J. Košík, A. Welle, J.M. Guigner, O. Clemens, G.E. Schaumann, Extraction and characterization methods for titanium dioxide nanoparticles from commercialized sunscreens, *Environ. Sci. Nano.* 5 (2018) 191–202. doi:10.1039/c7en00677b.
- [37] W. Dufefoi, H. Terrisse, A.F. Popa, E. Gautron, B. Humbert, M.H. Ropers, Evaluation of the content of TiO<sub>2</sub> nanoparticles in the coatings of chewing gums, *Food Addit. Contam. - Part A.* (2017) 1–11. doi:10.1080/19440049.2017.1384576.
- [38] X. Jiang, M. Manawan, T. Feng, R. Qian, T. Zhao, G. Zhou, F. Kong, Q. Wang, S. Dai, J.H. Pan, Anatase and rutile in evonik aerioxide P25: Heterojunctioned or individual nanoparticles?, *Catal. Today.* 300 (2018) 12–17. doi:10.1016/j.cattod.2017.06.010.
- [39] W. Dufefoi, H. Terrisse, M. Richard-Plouet, E. Gautron, F. Popa, B. Humbert, M.H. Ropers, Criteria to define a more relevant reference sample of titanium dioxide in the context of food: a multiscale approach, *Food Addit. Contam. - Part A.* (2017) 1–13. doi:10.1080/19440049.2017.1284346.
- [40] OECD, Case study on grouping and read-across for nanomaterials — genotoxicity of nano-TiO<sub>2</sub> (Series on Testing and Assessment No. 292), 2018. [http://www.oecd.org/officialdocuments/publicdisplaydocumentpdf/?cote=ENV/JM/MONO\(2018\)28&docLanguage=En](http://www.oecd.org/officialdocuments/publicdisplaydocumentpdf/?cote=ENV/JM/MONO(2018)28&docLanguage=En).
- [41] W. Sangchay, L. Sikong, K. Kooptarnond, Comparison of photocatalytic reaction of commercial P25 and synthetic TiO<sub>2</sub>-AgCl nanoparticles, *Procedia Eng.* 32 (2012) 590–596. doi:10.1016/j.proeng.2012.01.1313.
- [42] Dott. Marco Marchetti, Synthesis and chemical-physical characterization of photocatalytic inorganic nanocrystals for innovative technological applications, Università degli Studi di Bologna, 2013. [http://amsdottorato.unibo.it/5737/2/marchetti\\_marco\\_tesi.pdf](http://amsdottorato.unibo.it/5737/2/marchetti_marco_tesi.pdf).
- [43] A. Weir, P. Westerhoff, L. Fabricius, N. von Goetz, Titanium Dioxide Nanoparticles in Food and Personal Care Products, *Environ. Sci. Technol.* 46 (2012) 2242–2250. doi:10.1021/es204168d.

- [44] INRS guide Line, Nanomaterials, current situation and prospects in occupational health and safety, 2013. <https://www.inrs.fr/risques/nanomateriaux/travaux-inrs.html>.
- [45] A. Delvallée, N. Feltin, S. Ducourtieux, M. Trabelsi, J.F. Hochepped, Direct comparison of AFM and SEM measurements on the same set of nanoparticles, *Meas. Sci. Technol.* 26 (2015) 1–15. doi:10.1088/0957-0233/26/8/085601.
- [46] M. Bussiek, N. Mücke, J. Langowski, Polylysine-coated mica can be used to observe systematic changes in the supercoiled DNA conformation by scanning force microscopy in solution., *Nucleic Acids Res.* 31 (2003). doi:10.1093/nar/gng137.
- [47] O. Spalla, S. Lyonnard, F. Testard, Analysis of the small-angle intensity scattered by a porous and granular medium, *J. Appl. Crystallogr.* 36 (2003) 338–347. doi:10.1107/s0021889803002279.
- [48] J. Foucher, A. Labrosse, A. Dervillé, Y. Zimmermann, G. Bernard, S. Martinez, H. Grönqvist, J. Baderot, F. Pinzan, The coming of age of the first hybrid metrology software platform dedicated to nanotechnologies (Conference Presentation), in: *Soc. Photo-Optical Instrum. Eng.*, 2017. doi:10.1117/12.2258093.
- [49] H. Rauscher, A. Mech, C. Gaillard, M. Stintz, W. Wohlleben, S. Weigel, A. Ghanem, D. Hodoroaba, F. Babick, J. Mielke, Recommendations on a Revision of the EC Definition of Nanomaterial Based on Analytical Possibilities, 2015.
- [50] IRAMIS CEA SACLAY, SWAXS-Lab platform, (n.d.). [http://iramis.cea.fr/LIDYL/en/Phoce/Vie\\_des\\_labos/Ast/ast\\_sstechnique.php?id\\_ast=2729&voir=images](http://iramis.cea.fr/LIDYL/en/Phoce/Vie_des_labos/Ast/ast_sstechnique.php?id_ast=2729&voir=images).
- [51] CEA-IRAMIS-LIONS, Python for Small Angle X-ray Scattering data acquisition, treatment and computation of model SAXS intensities, (n.d.). <https://pypi.org/project/pySAXS/>.
- [52] O. Taché, S. Rouzière, P. Joly, M. Amara, B. Fleury, A. Thill, P. Launois, O. Spalla, B. Abécassis, MOMAC: A SAXS/WAXS laboratory instrument dedicated to nanomaterials, *J. Appl. Crystallogr.* 49 (2016) 1624–1631. doi:10.1107/S1600576716012127.
- [53] André Guinier, Gérard Fournet, and C. B. Walker, *Small-angle scattering of X-rays*, 1955. doi:10.1063/1.3060069.
- [54] T. Zemb, P. Lindner, *Neutrons, X-rays, and light : scattering methods applied to soft condensed matter*, 1st ed., Elsevier, 2002.
- [55] ISO 15901-3:2007 Pore size distribution and porosity of solid materials by mercury porosimetry and gas adsorption — Part 3: Analysis of micropores by gas adsorption, 2007. <https://www.iso.org/obp/ui/#iso:std:iso:15901:-3:ed-1:v1:en>.
- [56] ISO 9277:2010, Determination of the specific surface area of solids by gas adsorption — BET method, 2010. <https://www.iso.org/obp/ui/#iso:std:iso:9277:ed-2:v1:en>.
- [57] W. Wohlleben, J. Mielke, A. Bianchin, A. Ghanem, H. Freiburger, H. Rauscher, M. Gemeinert, V.D. Hodoroaba, Reliable nanomaterial classification of powders using the volume-specific surface area method, *J. Nanoparticle Res.* 19 (2017) 1–16. doi:10.1007/s11051-017-3741-x.
- [58] F.T.L. Muniz, M.A.R. Miranda, C. Morilla Dos Santos, J.M. Sasaki, The Scherrer equation and the dynamical theory of X-ray diffraction, *Acta Crystallogr. Sect. A Found. Adv.* 72 (2016) 385–

390. doi:10.1107/S205327331600365X.

- [59] A.O.T. Patrocínio, E.B. Paniago, R.M. Paniago, N.Y.M. Iha, XPS characterization of sensitized n-TiO<sub>2</sub> thin films for dye-sensitized solar cell applications, *Appl. Surf. Sci.* 254 (2008) 1874–1879. doi:10.1016/j.apsusc.2007.07.185.
- [60] V.G. Bessergenev, M.C. Mateus, A.M. Botelho Do Rego, M. Hantusch, E. Burkel, An improvement of photocatalytic activity of TiO<sub>2</sub> Degussa P25 powder, *Appl. Catal. A Gen.* 500 (2015) 40–50. doi:10.1016/j.apcata.2015.05.002.
- [61] Y. Yang, D. Kyle, X. Bi, K. Hristovski, P. Herckes, P. Westerhoff, R. Kaegi, Characterization of Food-Grade Titanium Dioxide: The Presence of Nanosized Particles, *Environ. Sci. Technol.* 48 (2014) 6391–6400. doi:10.1021/es500436x.
- [62] N. Serpone, D. Dondi, A. Albini, Inorganic and organic UV filters: Their role and efficacy in sunscreens and suncare products, *Inorganica Chim. Acta.* 360 (2007) 794–802. doi:10.1016/j.ica.2005.12.057.
- [63] W. Dufefoi, Titanium dioxide particles in food: characterization, fate in digestive fluids and impact on human gut microbiota, l'Université de Nantes sous le sceau de l'Université Bretagne Loire, 2017.
- [64] O. Geiss, J. Ponti, C. Senaldi, I. Bianchi, D. Mehn, J. Barrero, D. Gilliland, R. Matissek, E. Anklam, Characterisation of food grade titania with respect to nanoparticle content in pristine additives and in their related food products, *Food Addit. Contam. - Part A.* 37 (2020) 239–253. doi:10.1080/19440049.2019.1695067.
- [65] M. Kosmulski, Compilation of PZC and IEP of sparingly soluble metal oxides and hydroxides from literature, *Adv. Colloid Interface Sci.* 152 (2009) 14–25. doi:10.1016/j.cis.2009.08.003.
- [66] R.A. Spurr, H. Myers, Quantitative Analysis of Anatase-Rutile Mixtures with an X-Ray Diffractometer, *Anal. Chem.* 29 (1957) 760–762. doi:10.1021/ac60125a006.
- [67] J.F. Porter, Y.-G. Li, C.K. Chan, The effect of calcination on the microstructural characteristics and photoreactivity of Degussa P-25 TiO<sub>2</sub>, *J. Mater. Sci.* 34 (1999) 1523–1531. doi:10.1023/A:1004560129347.
- [68] S. Bakardjieva, J. Šubrt, V. Štengl, M.J. Dianez, M.J. Sayagues, Photoactivity of anatase-rutile TiO<sub>2</sub> nanocrystalline mixtures obtained by heat treatment of homogeneously precipitated anatase, *Appl. Catal. B Environ.* 58 (2005) 193–202. doi:10.1016/j.apcatb.2004.06.019.
- [69] J. Yu, H. Yu, B. Cheng, M. Zhou, X. Zhao, Enhanced photocatalytic activity of TiO<sub>2</sub> powder (P25) by hydrothermal treatment, *J. Mol. Catal. A Chem.* 253 (2006) 112–118. doi:10.1016/j.molcata.2006.03.021.
- [70] B. Ohtani, O.O. Prieto-Mahaney, D. Li, R. Abe, What is Degussa (Evonic) P25? Crystalline composition analysis, reconstruction from isolated pure particles and photocatalytic activity test, *J. Photochem. Photobiol. A Chem.* 216 (2010) 179–182. doi:10.1016/j.jphotochem.2010.07.024.
- [71] M. Motzkus, C. Macé, T. Vaslin Reimann, S. Ausset, P. Maillé, Characterization of manufactured TiO<sub>2</sub> nanoparticles, *J. Phys. Conf. Ser.* 429 (2013) 1–10. doi:10.1088/1742-6596/429/1/012012.

- [72] J.J. Faust, K. Doudrick, Y. Yang, D.G. Capco, P. Westerhoff, A facile method for separating and enriching nano and submicron particles from titanium dioxide found in food and pharmaceutical products, *PLoS One*. 11 (2016) 1–15. doi:10.1371/journal.pone.0164712.
- [73] X. Guo, A. Gutsche, M. Wagner, M. Seipenbusch, H. Nirschl, Simultaneous SWAXS study of metallic and oxide nanostructured particles, *J. Nanoparticle Res.* 15 (2013). doi:10.1007/s11051-013-1559-8.
- [74] B. Viswanathan, K.J.A. Raj, Effect of surface area, pore volume and particle size of P25 titania on the phase transformation of anatase to rutile, *Indian J. Chem. - Sect. A Inorganic, Phys. Theor. Anal. Chem.* 48 (2009) 1378–1382.
- [75] C. Motzkus, T. Macé, F. Gaie-Levrel, S. Ducourtieux, A. Delvallee, K. Dirscherl, V.-D. Hodoroaba, I. Popov, O. Popov, I. Kuselman, K. Takahata, K. Ehara, P. Ausset, M. Maillé, N. Michielsen, S. Bondiguel, F. Gensdarmes, L. Morawska, G.R. Johnson, E.M. Faghihi, C.S. Kim, Y.H. Kim, M.C. Chu, J.A. Guardado, A. Salas, G. Capannelli, C. Costa, T. Bostrom, Å.K. Jämting, M.A. Lawn, L. Adlem, S. Vaslin-Reimann, Size characterization of airborne SiO<sub>2</sub> nanoparticles with on-line and off-line measurement techniques: an interlaboratory comparison study, *J. Nanoparticle Res.* 15 (2013). doi:10.1007/s11051-013-1919-4.
- [76] J.M. Teulon, C. Godon, L. Chantalat, C. Moriscot, J. Cambedouzou, M. Odorico, J. Ravaux, R. Podor, A. Gerdil, A. Habert, N. Herlin-Boime, S.W.W. Chen, J.L. Pellequer, On the operational aspects of measuring nanoparticle sizes, *Nanomaterials*. 9 (2019) 1–29. doi:10.3390/nano9010018.
- [77] A. Deschamps, F. De Geuser, On the validity of simple precipitate size measurements by small-angle scattering in metallic systems, *J. Appl. Crystallogr.* 44 (2011) 343–352. doi:10.1107/S0021889811003049.